iScience, Volume *23*

Supplemental Information

Phosphoglycerate Mutase Cooperates with Chk1 Kinase to Regulate Glycolysis

Takumi Mikawa, Eri Shibata, Midori Shimada, Ken Ito, Tomiko Ito, Hiroaki Kanda, Keiyo Takubo, Matilde E. Lleonart, Nobuya Inagaki, Masayuki Yokode, and Hiroshi Kondoh

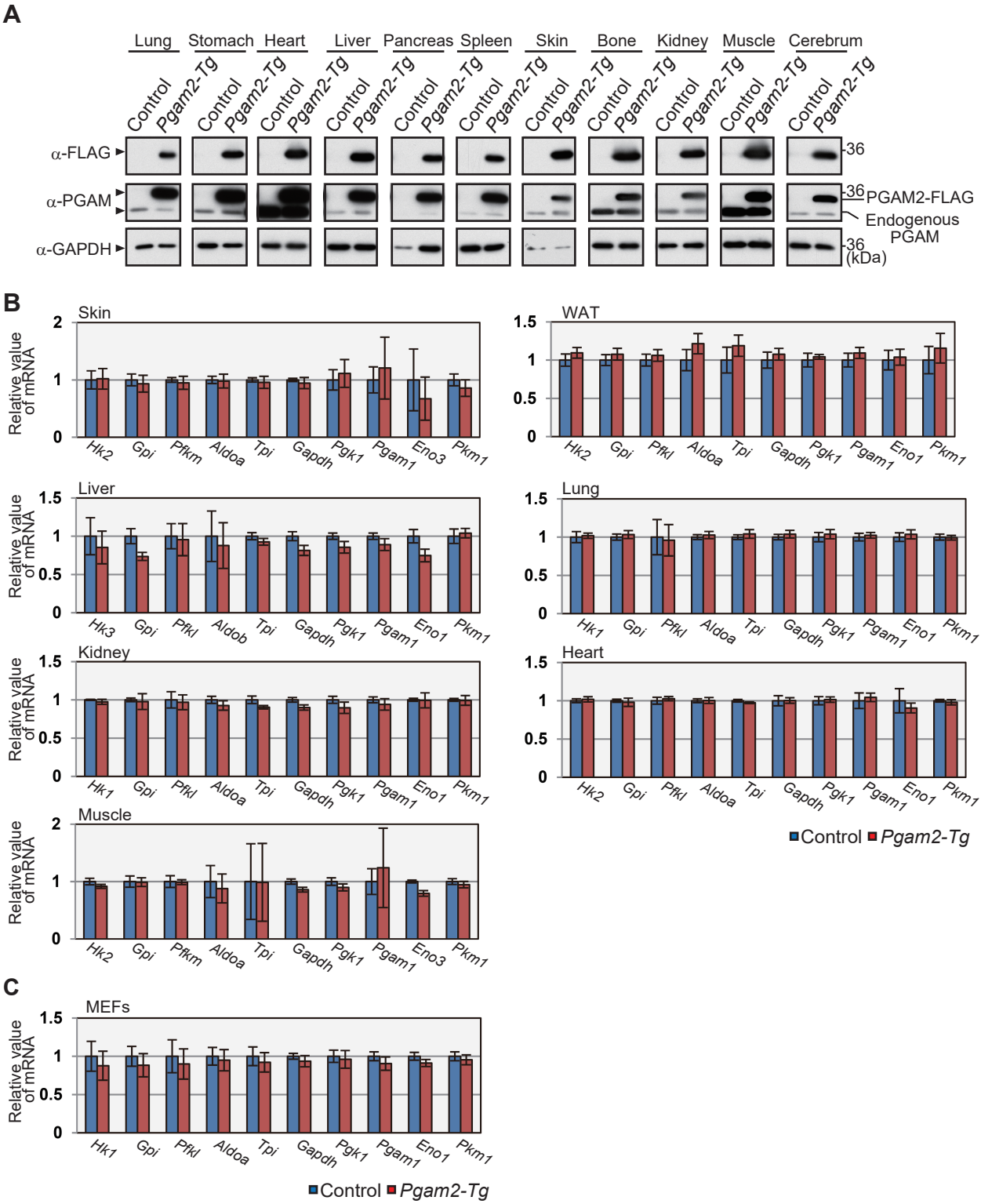
A
Lung
Stomach
Heart
Liver
Pancreas
Spleen
Skin
Bone
Kidney
Muscle
Cerebrum
Control
Pgam2-Tg
α-FLAG
α-PGAM
α-GAPDH
36
PGAM2-FLAG
Endogenous PGAM
(kDa)
B
Skin
WAT
Liver
Lung
Kidney
Heart
Muscle
Relative value of mRNA
Hk2 Gpi Pfkm Aldoa Tpi Gapdh Pgk1 Pgam1 Eno3 Pkm1
Hk2 Gpi Pfkl Aldoa Tpi Gapdh Pgk1 Pgam1 Eno1 Pkm1
Hk3 Gpi Pfkl Aldob Tpi Gapdh Pgk1 Pgam1 Eno1 Pkm1
Hk1 Gpi Pfkl Aldoa Tpi Gapdh Pgk1 Pgam1 Eno1 Pkm1
Hk2 Gpi Pfkm Aldoa Tpi Gapdh Pgk1 Pgam1 Eno3 Pkm1
Control
Pgam2-Tg
C
MEFs
Hk1 Gpi Pfkl Aldoa Tpi Gapdh Pgk1 Pgam1 Eno1 Pkm1
Control
Pgam2-Tg

Figure S1. Glycolytic profiles in *Pgam2-Tg* mice. Related to Figure 1

(A) Ectopic expression of PGAM2-FLAG was detected by immunoblotting in various tissues from control (wild-type) and *Pgam2-Tg* mice. Anti-FLAG, anti-PGAM, and anti-GAPDH antibodies were used. **(B)** Relative mRNA levels for glycolytic enzymes in control (WT; *n* = 4) and *Pgam2-Tg* (*n* = 4) mice. Total RNA was extracted from various tissues, including skin, liver, kidney, muscle, white adipose tissue (WAT), lung, and heart. **(C)** Relative mRNA levels for glycolytic enzymes in control (*n* = 3) and *Pgam2-Tg* MEFs (*n* = 3). Data are relative to those expressed in control. *Hk1*: hexokinase1; *Hk2*: hexokinase2; *Hk3*: hexokinase3; *Gpi*: glucose phosphate isomerase; *Pfkl*: phosphofructokinase L; *Pfkm*: phosphofructokinase M; *Aldoa*: aldolase A; *Aldob*: aldolase B;*Tpi*: triose phosphate isomerase; *Gapdh*: glyceraldehyde 3-phosphate dehydrogenase; *Pgk1*: phosphoglycerate kinase1; *Pgam1*: phosphoglycerate mutase1;*Eno1*: enolase1; *Eno3*: enolase3; *Pkm1*: pyruvate kinase M1.

A

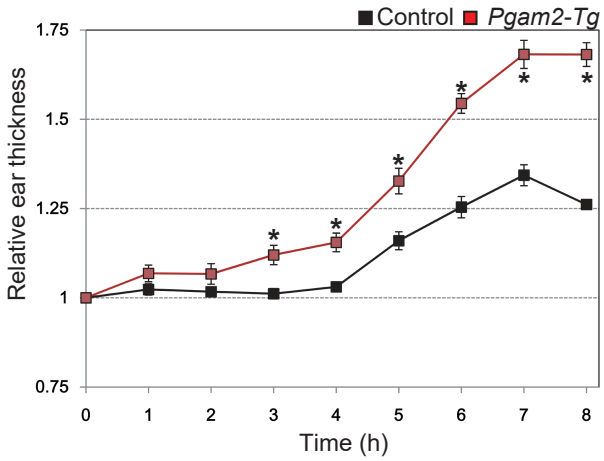
Control
Pgam2-Tg
Relative ear thickness
1.75
1.5
1.25
1
0.75
0
1
2
3
4
5
6
7
8
Time (h)
*

B


Control
Pgam2-Tg

C

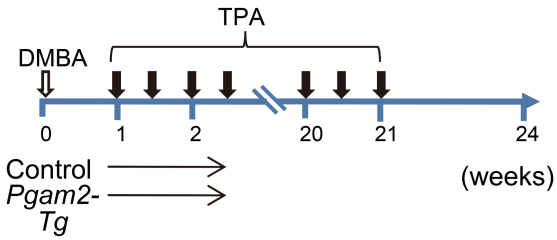
TPA
DMBA
0
1
2
20
21
24
Control
Pgam2-Tg
(weeks)

D

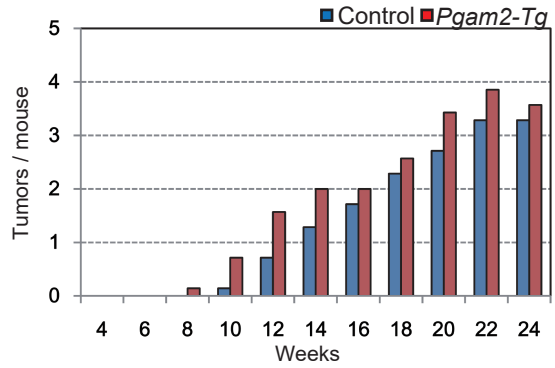
Control
Pgam2-Tg
Tumors / mouse
5
4
3
2
1
0
4
6
8
10
12
14
16
18
20
22
24
Weeks

Figure S2. TPA-induced skin inflammation and chemically induced tumorigenesis in *Pgam2-Tg* mice. Related to Figure 1

(A-B) Comparison of proinflammatory TPA-treated ears between control (wild-type) (n=3) and *Pgam2-Tg* mice (n=3). **(A)** Mice at 35 weeks were treated with 10 ng TPA on the ears whose thickness were monitored for 8 hours. **(B)** Representative pictures of TPA-treated ears in control and *Pgam2-Tg* mice. **P*<0.05, Student's t-test. Data represent the mean ± SEM. **(C)** Schematic of the chemically-induced skin tumorigenesis protocol. Mice were treated with DMBA on Day 0, followed by treatment with TPA twice a week for 20 weeks. Histological examination of tumors was performed at 24 weeks. **(D)** Summary of total tumors during the protocol.

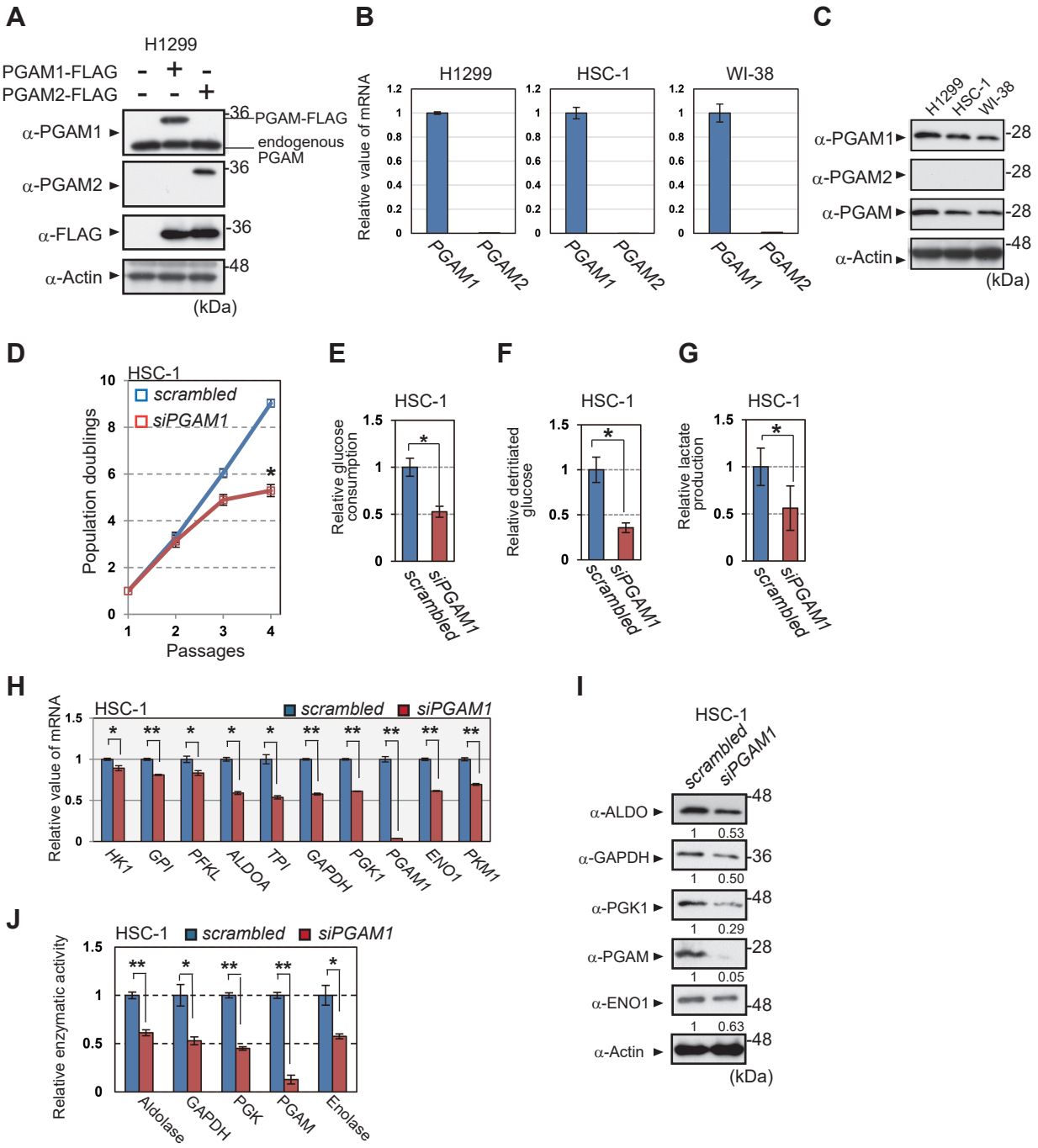
A
H1299
PGAM1-FLAG - + -
PGAM2-FLAG - - +
α-PGAM1
α-PGAM2
α-FLAG
α-Actin
36
PGAM-FLAG
endogenous PGAM
36
36
48
(kDa)
B
H1299
HSC-1
WI-38
Relative value of mRNA
PGAM1
PGAM2
C
H1299
HSC-1
WI-38
α-PGAM1
α-PGAM2
α-PGAM
α-Actin
28
28
28
48
(kDa)
D
HSC-1
scrambled
siPGAM1
Population doublings
Passages
E
HSC-1
Relative glucose consumption
siPGAM1
scrambled
F
HSC-1
Relative detritiated glucose
siPGAM1
scrambled
G
HSC-1
Relative lactate production
siPGAM1
scrambled
H
HSC-1
scrambled
siPGAM1
Relative value of mRNA
HK1
GPI
PFKL
ALDOA
TPI
GAPDH
PGK1
PGAM1
ENO1
PKM1
I
HSC-1
scrambled
siPGAM1
α-ALDO
α-GAPDH
α-PGK1
α-PGAM
α-ENO1
α-Actin
48
1 0.53
36
1 0.50
48
1 0.29
28
1 0.05
48
1 0.63
48
(kDa)
J
HSC-1
scrambled
siPGAM1
Relative enzymatic activity
Aldolase
GAPDH
PGK
PGAM
Enolase

Figure S3. Abrogation of PGAM inHSC-1 cells. Related to Figure 2

(A-C) The profiles of PGAM isoforms in H1299, HSC-1, and WI-38 cells. **(A)** Validation of antibodies against PGAM1 and 2. Western blotting was performed using the extracts from the transfected cells with indicated plasmids. Antibodies against PGAM1 (Abcam, ab129191) or PGAM2 (Abcam, ab183027) were applied. **(B)** The mRNA profiles of PGAM isoforms in indicated cells were evaluated by RT-PCR. **(C)** The protein profiles of PGAM isoforms in indicated cells. Anti PGAM antibody detects both isoforms, while anti PGAM1 or PGAM2 antibody detects relevant isoforms, as shown in panel (A). **(D-J)** The impact of *PGAM1* knockdown in HSC-1 cells *in vitro*. HSC-1 cells were transfected with *siPGAM1* (n=3) or scrambled RNA (n=3). **(D)** The proliferation curves of *PGAM1*-knockdown HSC-1 cells. Cells were passaged according to 3T3 cell culture protocol. **(E-I)** The glycolytic profiles were evaluated in *PGAM1*-knockdown HSC-1 cells. Glucose consumption was evaluated by measuring glucose concentration in medium **(E)**, whereas glycolytic flux was evaluated using ^{3}H-labeled glucose **(F)**. Lactate production was determined by the measurements of lactate concentration in medium **(G)**. **(H and I)** The mRNA and protein levels for glycolytic enzymes were assessed. The protein levels of the indicated glycolytic enzymes were analyzed by immunoblot (I). **(J)** Enzymatic activity of aldolase, GAPDH, PGK, PGAM and enolase was measured by spectrometric assay. *P < 0.05 and **P < 0.005, Student's t-test.

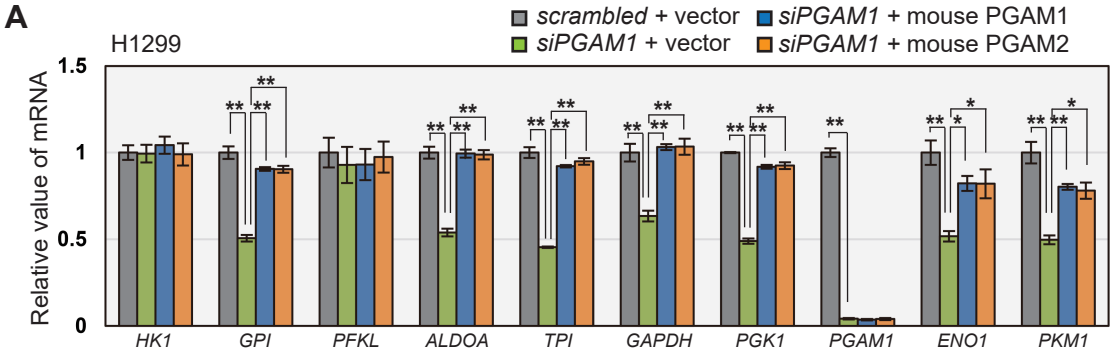
A
H1299
scrambled + vector
siPGAM1 + vector
siPGAM1 + mouse PGAM1
siPGAM1 + mouse PGAM2
Relative value of mRNA
HK1
GPI
PFKL
ALDOA
TPI
GAPDH
PGK1
PGAM1
ENO1
PKM1

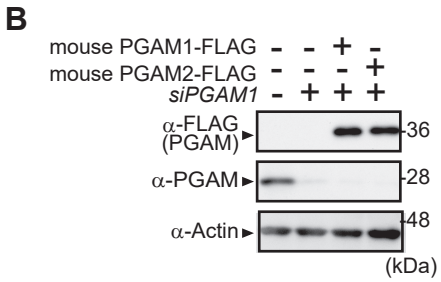
B
mouse PGAM1-FLAG
mouse PGAM2-FLAG
siPGAM1
α-FLAG (PGAM)
α-PGAM
α-Actin
36
28
48
(kDa)

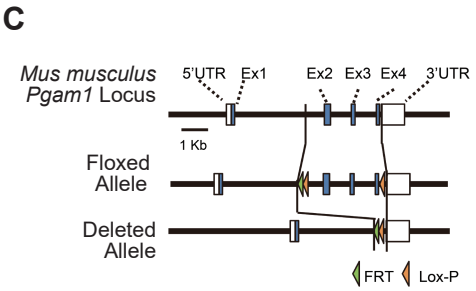
C
Mus musculus Pgam1 Locus
5'UTR
Ex1
Ex2
Ex3
Ex4
3'UTR
1 Kb
Floxed Allele
Deleted Allele
FRT
Lox-P

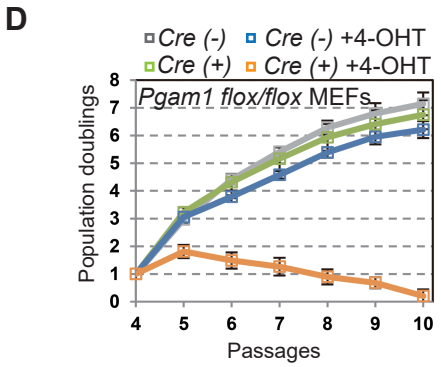
D
Cre (-)
Cre (-) +4-OHT
Cre (+)
Cre (+) +4-OHT
Pgam1 flox/flox MEFs
Population doublings
Passages

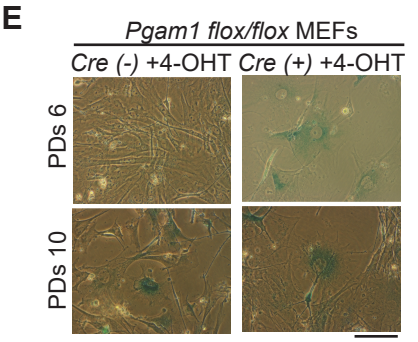
E
Pgam1 flox/flox MEFs
Cre (-) +4-OHT
Cre (+) +4-OHT
PDs 6
PDs 10

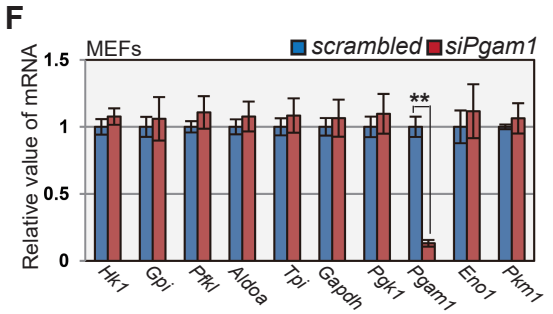
F
MEFs
scrambled
siPgam1
Relative value of mRNA
Hk1
Gpi
Pfkl
Aldoa
Tpi
Gapdh
Pgk1
Pgam1
Eno1
Pkm1

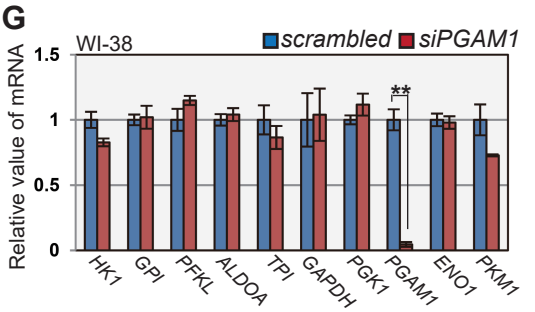
G
WI-38
scrambled
siPGAM1
Relative value of mRNA
HK1
GPI
PFKL
ALDOA
TPI
GAPDH
PGK1
PGAM1
ENO1
PKM1

Figure S4. Abrogation of PGAM in H1299 and standard cells.
Related to Figure 2

(A-B) H1299 cells with retroviral expression of empty vector, mouse PGAM1-FLAG, or mouse PGAM2-FLAG were prepared. Indicated cells were transfected with siRNA against endogenous human *PGAM1* or *scrambled* RNA. **(A)** The levels of glycolytic mRNAs were evaluated (n = 3). *P < 0.05 and **P < 0.005, Dunnett's multiple comparison test. **(B)** Immunoblotting detected both ectopically-expressed mouse PGAM-FLAG and endogenous human PGAM proteins in the indicated cells. **(C)** Construction of *Pgam1*-conditional KO mice is illustrated by a schematic diagram of the wild-type (WT), floxed, and *Pgam1* (exon 2–4) deleted alleles. **(D and E)** *Pgam1*$^{flox/flox}$ MEFs with or without *Cre-ER* were treated with 4-OHT, followed by serial passages according to the 3T3 cell culture protocol. *Cre (−)* and *(+)* indicate *Pgam1*$^{flox/flox}$ MEFs without or with *Cre-ER*, respectively. **(D)** Growth curves of indicated cells during 3T3 protocol. **(E)** SA-β-Gal staining was performed at passage 6 (PD6) and passage 10 (PD10) in *Pgam1* ablated MEFs (*Pgam1*$^{flox/flox}$ + *Cre-ER* with 4OHT) or control MEFs (*Pgam1*$^{flox/flox}$ with 4OHT). Scale bar indicates 200 μm. **(F and G)** Levels of glycolytic mRNAs in *siPgam1*-transfected standard cells. Primary MEFs **(F)** or human WI-38 **(G)** cells were prepared. Data are relative to expression in cells transfected with scrambled RNA. *P < 0.05 and **P < 0.005, Student's t-test. Data represent the mean ± SEM.

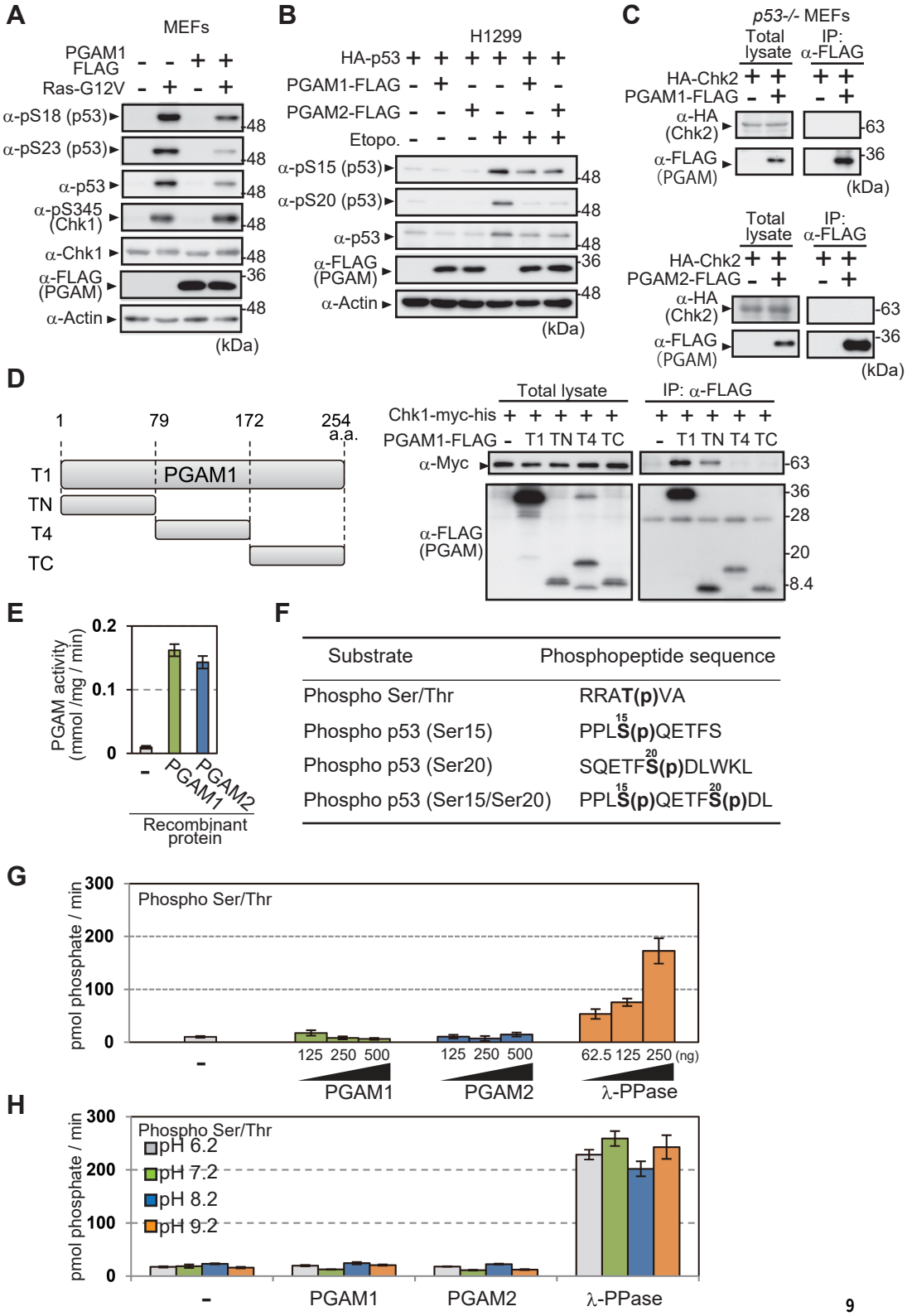
A
MEFs
PGAM1 FLAG - - + +
Ras-G12V - + - +
α-pS18 (p53)
α-pS23 (p53)
α-p53
α-pS345 (Chk1)
α-Chk1
α-FLAG (PGAM)
α-Actin
48
36
(kDa)
B
H1299
HA-p53 + + + + + +
PGAM1-FLAG - + - - + -
PGAM2-FLAG - - + - - +
Etopo. - - - + + +
α-pS15 (p53)
α-pS20 (p53)
α-p53
α-FLAG (PGAM)
α-Actin
48
36
(kDa)
C
p53-/- MEFs
Total lysate
IP: α-FLAG
HA-Chk2 + + + +
PGAM1-FLAG - + - +
α-HA (Chk2)
α-FLAG (PGAM)
63
36
(kDa)
Total lysate
IP: α-FLAG
HA-Chk2 + + + +
PGAM2-FLAG - + - +
α-HA (Chk2)
α-FLAG (PGAM)
63
36
(kDa)
D
1
79
172
254 a.a.
T1
TN
T4
TC
PGAM1
Total lysate
IP: α-FLAG
Chk1-myc-his + + + + + + + + + +
PGAM1-FLAG - T1 TN T4 TC - T1 TN T4 TC
α-Myc
α-FLAG (PGAM)
63
36
28
20
8.4
E
PGAM activity (mmol /mg / min)
0.2
0.1
0
-
PGAM1
PGAM2
Recombinant protein
F
Substrate | Phosphopeptide sequence
Phospho Ser/Thr | RRAT(p)VA
Phospho p53 (Ser15) | PPLS15(p)QETFS
Phospho p53 (Ser20) | SQETFS20(p)DLWKL
Phospho p53 (Ser15/Ser20) | PPLS15(p)QETFS20(p)DL
G
pmol phosphate / min
300
200
100
0
Phospho Ser/Thr
-
125 250 500
PGAM1
125 250 500
PGAM2
62.5 125 250 (ng)
λ-PPase
H
pmol phosphate / min
300
200
100
0
Phospho Ser/Thr
pH 6.2
pH 7.2
pH 8.2
pH 9.2
-
PGAM1
PGAM2
λ-PPase

Figure S5. The impact of PGAM on p53 phosphorylation and the assessment of protein phosphatase activity of PGAM. Related to Figure 3

(A-B) The impact of PGAM on the phosphorylation status of p53 was evaluated by western blotting. Primary MEFs were stressed by oncogenic Ras-G12V expression (A), while H1299 cells with indicated plasmids were treated with 100 μM Etoposide for 3 h (B). **(C)** The interaction between PGAM and Chk2 was examined in *p53*$^{-/-}$ MEFs transfected with HA-Chk2 and PGAM1- or 2-FLAG (upper and lower panels, respectively). **(D)** The evaluation of the interaction between Chk1 and various versions of PGAM1-FLAG. Left panel shows schematic diagram of various fragments of PGAM1. The binding of each fragment to Chk1 was assessed by co-immunoprecipitation (right panels). Extracts from *p53*$^{-/-}$ MEFs transfected with the indicated plasmids were immunoprecipitated with an anti-FLAG antibody. **(E)** Assessment of enzymatic activity for recombinant PGAM1 and PGAM2 protein. **(F)** The sequence of the phosphopeptides used for the *in vitro* phosphatase assay. RRAT(p)VA phosphopeptide (Phospho Ser/Thr) is compatible as a substrate for several serine/threonine phosphatases such as protein phosphatases 2A, 2B, and 2C. Phospho p53 (Ser15, Ser20, and Ser15/Ser20) phosphopeptides mimicked the p53 fragment phosphorylated at Ser15, Ser20, or Ser15/Ser20, respectively. **(G and H)** Phosphatase activity of recombinant PGAM1 and PGAM2 was evaluated. 5000 pmol phosphopeptides were incubated with recombinant PGAM1, PGAM2, or λPPase for 30 min, and the amount of released phosphate from phosphopeptides was monitored. **(G)** Phosphatase activity against phospho-Ser/Thr peptides was assessed with increasing amounts of recombinant PGAM (125, 250, and 500 ng) or λPPase (62.5, 125, and 250 ng). **(H)** Phosphatase activity against phospho-Ser/Thr peptides was assessed using 500 ng PGAM1 or PGAM2, or 250 ng λPPase in the indicated pH conditions. Data represent the mean ± SEM.

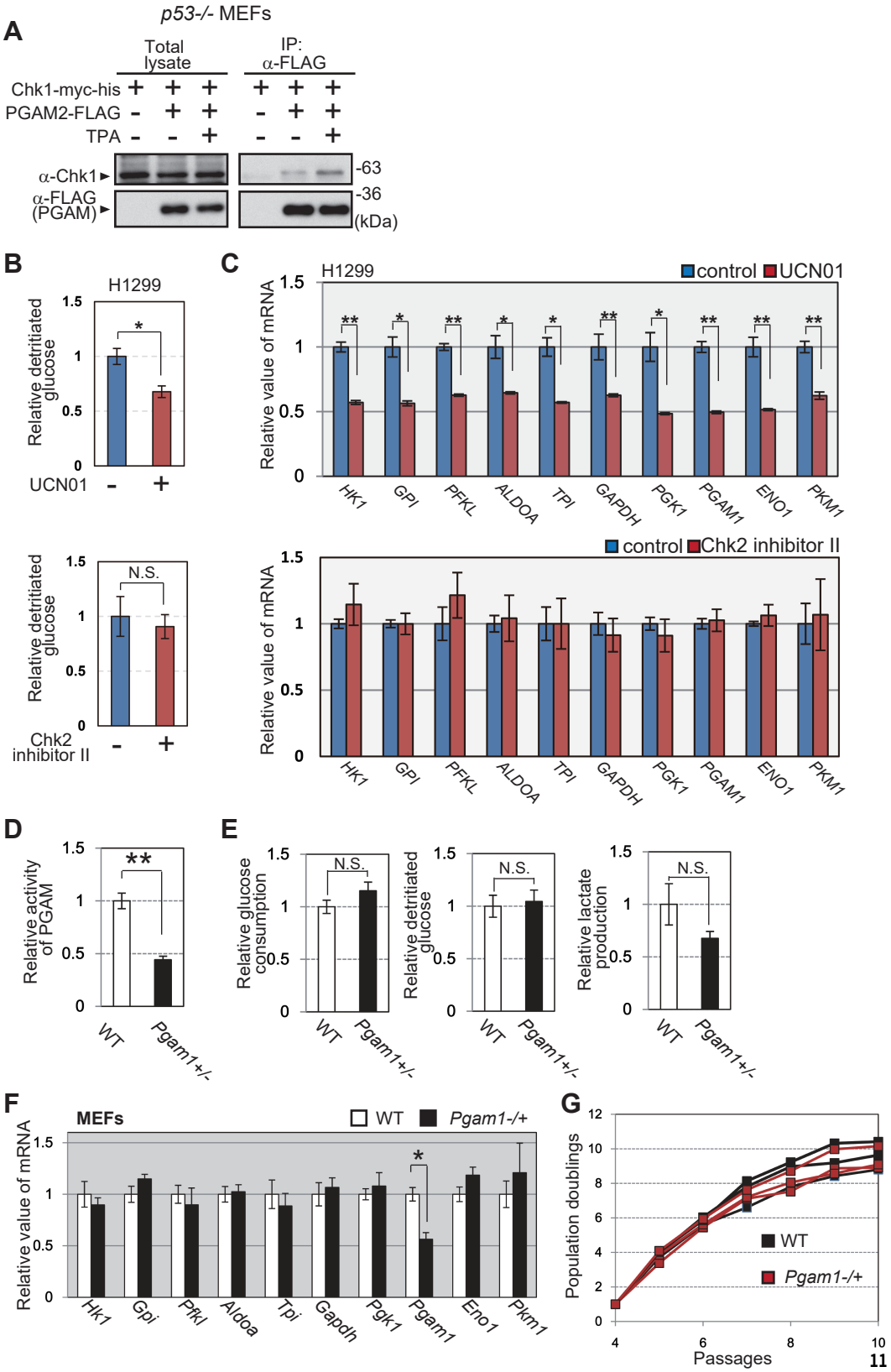
A
p53-/- MEFs
Total lysate
IP: α-FLAG
Chk1-myc-his + + + + + +
PGAM2-FLAG - + + - + +
TPA - - + - - +
α-Chk1
α-FLAG (PGAM)
-63
-36
(kDa)
B
H1299
Relative detritiated glucose
UCN01 - +
N.S.
Chk2 inhibitor II - +
C
H1299
control UCN01
Relative value of mRNA
HK1 GPI PFKL ALDOA TPI GAPDH PGK1 PGAM1 ENO1 PKM1
control Chk2 inhibitor II
D
Relative activity of PGAM
WT Pgam1+/-
E
Relative glucose consumption
Relative detritiated glucose
Relative lactate production
N.S.
F
MEFs
WT Pgam1-/+
Relative value of mRNA
Hk1 Gpi Pfkl Aldoa Tpi Gapdh Pgk1 Pgam1 Eno1 Pkm1
G
Population doublings
Passages
WT
Pgam1-/+

Figure S6. Impact of Chk1 on glycolytic mRNAs. Related to Figure 4

(A) The impact of TPA treatment on the interaction between PGAM and Chk1. $p53^{-/-}$ MEFs with expression of Chk1-myc-his and PGAM2-FLAG were treated with or without 0.1 μg/ml TPA for 48 hours, followed by treatment with MG132 for 3 h. The cell lysates were immunoprecipitated with an anti-FLAG antibody. **(B and C)** Effect of UCN01 (Chk1 inhibitor) or Chk2-inhibitor II on glycolytic profiles in H1299 cells (*n* = 3). H1299 were exposed to 500 nM UCN01 or 10 μM Chk2 inhibitor II for 12 h (upper and lower panel, respectively). **(B)** Glycolytic flux was evaluated in indicated cells (n=3). **(C)** The glycolytic mRNA expression was detected by qRT-PCR. Data are relative to expression in control cells. **P* < 0.05 and ***P* < 0.005, Student's t-test. **(D-G)** Cytological characterization of *Pgam1* heterozygous KO MEFs. **(D)** Measurement of total PGAM enzymatic activity in WT (*n* = 3) and $Pgam1^{+/-}$ MEFs (*n* = 3). **(E)** Glucose consumption (left), glucose flux (middle), and lactate production (right) in WT (*n* = 3) or $Pgam1^{+/-}$ MEFs (*n* = 3). **(F)** Comparison of glycolytic mRNAs by real-time qRT-PCR between wild-type (WT) (*n* = 3) and $Pgam1^{+/-}$ MEFs (*n* = 3). Data are shown as relative values against those in WT. **(G)** Growth curves of WT and $Pgam1^{+/-}$ MEFs Three independent lines of each MEF were passaged according to 3T3 cell culture protocol. **P* < 0.05 and ***P* < 0.005, Student's t-test. Data represent the mean ± SEM.

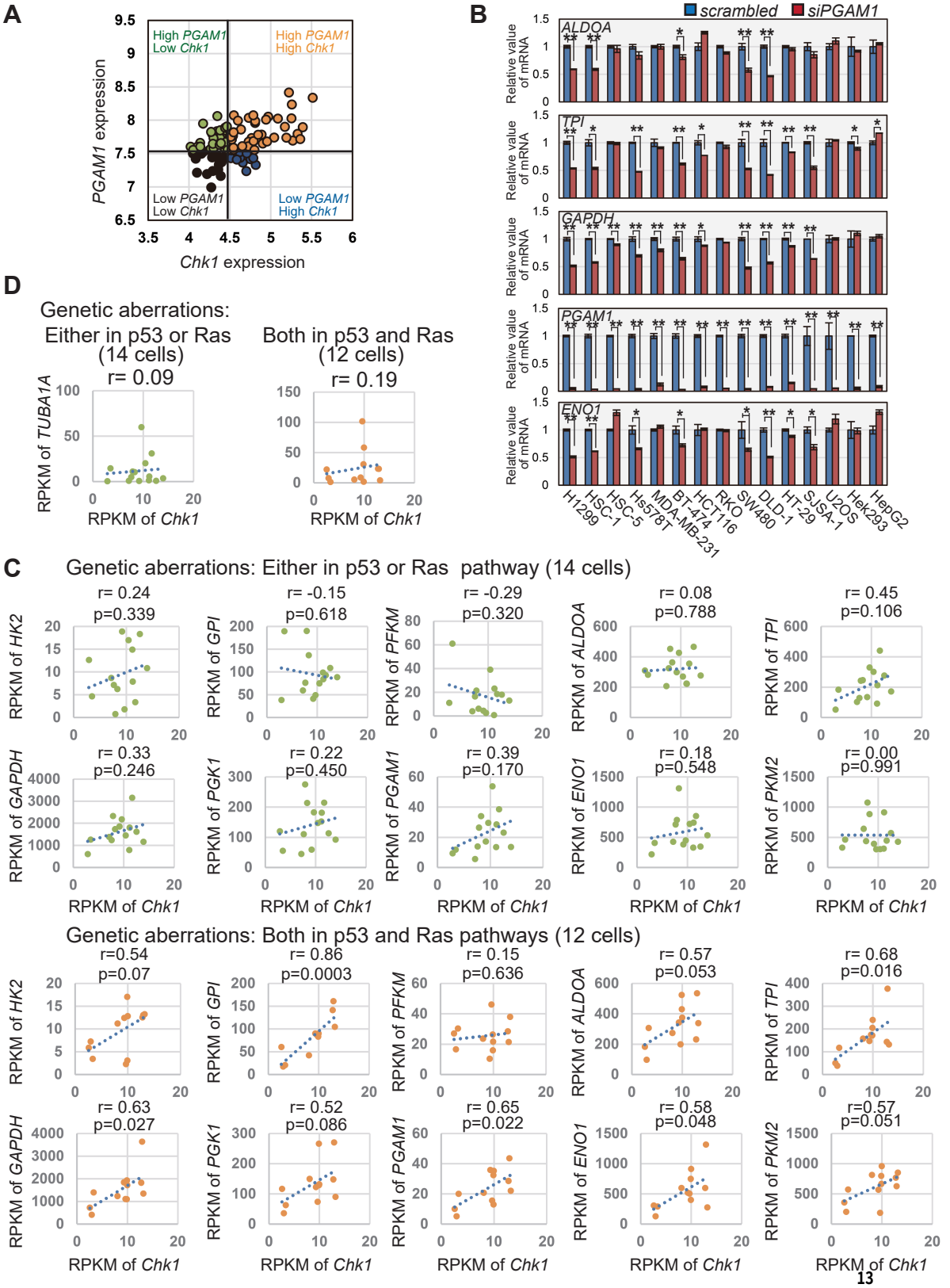
A
High PGAM1
Low Chk1
High PGAM1
High Chk1
Low PGAM1
Low Chk1
Low PGAM1
High Chk1
PGAM1 expression
Chk1 expression
B
scrambled
siPGAM1
ALDOA
TPI
GAPDH
PGAM1
ENO1
Relative value of mRNA
H1299
HSC-1
HSC-5
Hs578T
MDA-MB-231
BT-474
HCT116
RKO
SW480
DLD-1
HT-29
SUSA-1
U2OS
Hek293
HepG2
D
Genetic aberrations:
Either in p53 or Ras (14 cells)
r= 0.09
Both in p53 and Ras (12 cells)
r= 0.19
RPKM of TUBA1A
RPKM of Chk1
C
Genetic aberrations: Either in p53 or Ras pathway (14 cells)
r= 0.24
p=0.339
r= -0.15
p=0.618
r= -0.29
p=0.320
r= 0.08
p=0.788
r= 0.45
p=0.106
RPKM of HK2
RPKM of GPI
RPKM of PFKM
RPKM of ALDOA
RPKM of TPI
r= 0.33
p=0.246
r= 0.22
p=0.450
r= 0.39
p=0.170
r= 0.18
p=0.548
r= 0.00
p=0.991
RPKM of GAPDH
RPKM of PGK1
RPKM of PGAM1
RPKM of ENO1
RPKM of PKM2
RPKM of Chk1
Genetic aberrations: Both in p53 and Ras pathways (12 cells)
r=0.54
p=0.07
r= 0.86
p=0.0003
r= 0.15
p=0.636
r= 0.57
p=0.053
r= 0.68
p=0.016
r= 0.63
p=0.027
r= 0.52
p=0.086
r= 0.65
p=0.022
r= 0.58
p=0.048
r=0.57
p=0.051

Figure S7. Analysis of patient prognosis and cell lines for lung cancer. Related to Figure 5

(A) The comparison plot for *PGAM1* and *Chk1* levels in 104 NSCLC patients (Dataset Jacob-00182-MSK). According to the expression levels of *PGAM1* or *Chk1*, NSCLC patients were categorized into four groups, as shown in Figure 5A. Cut-off points for *PGAM1* and *Chk1* were 7.546 and 4.509, respectively. **(B)** The levels of the glycolytic mRNAs, *ALDO1, TPI, GAPDH* and *ENO1*, were evaluated in *PGAM1*-knockdown cancer cell lines (n = 3 per cell line). Values for indicated targets are relative to those in cells transfected with scrambled siRNA. *P < 0.05 and **P < 0.005, Student's t-test. **(C and D)** Association of expression levels among indicated genes was evaluated in dataset of 26 non-small cell lung adenocarcinoma cell lines as shown in Figure 5C. **(C)** Association between *Chk1* and glycolytic enzymes in two indicated subgroups; 14 cells with genetic aberration either in p53 or Ras pathway, and 12 cells mutated in both. **(D)** Association between expressions of *Chk1* and *TUBA1A*. Correlation-coefficient and significance-probability were presented as r-value and p-value, respectively.

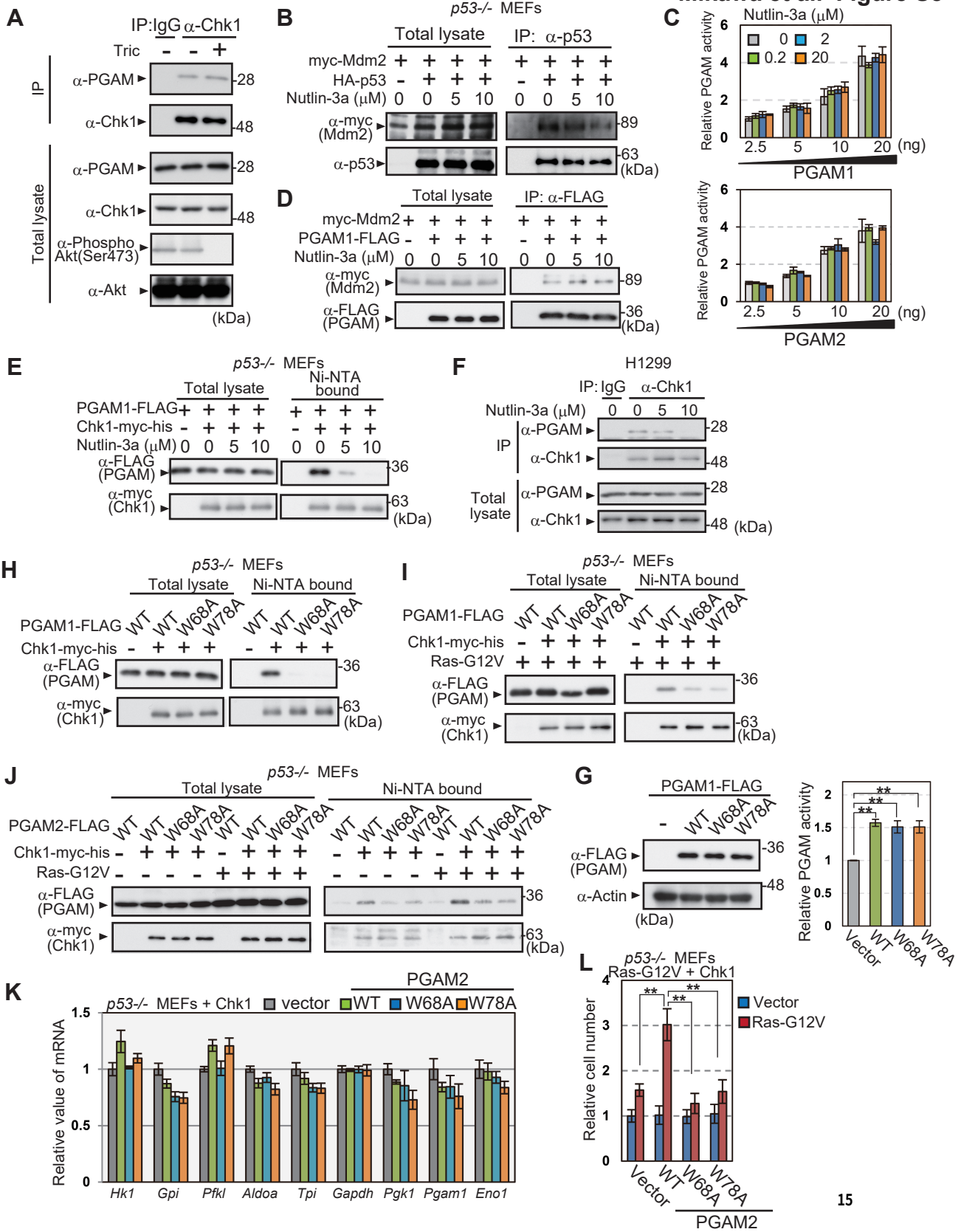
A
IP:IgG α-Chk1
Tric - - +
IP
α-PGAM
28
α-Chk1
48
Total lysate
α-PGAM
28
α-Chk1
48
α-Phospho Akt(Ser473)
α-Akt
(kDa)
B
p53-/- MEFs
Total lysate
IP: α-p53
myc-Mdm2 + + + + + + + +
HA-p53 - + + + - + + +
Nutlin-3a (μM) 0 0 5 10 0 0 5 10
α-myc (Mdm2)
89
α-p53
63
(kDa)
C
Nutlin-3a (μM)
0 2 0.2 20
Relative PGAM activity
2.5 5 10 20 (ng)
PGAM1
PGAM2
D
Total lysate
IP: α-FLAG
myc-Mdm2 + + + + + + + +
PGAM1-FLAG - + + + - + + +
Nutlin-3a (μM) 0 0 5 10 0 0 5 10
α-myc (Mdm2)
89
α-FLAG (PGAM)
36
(kDa)
E
p53-/- MEFs
Total lysate
Ni-NTA bound
PGAM1-FLAG + + + + + + + +
Chk1-myc-his - + + + - + + +
Nutlin-3a (μM) 0 0 5 10 0 0 5 10
α-FLAG (PGAM)
36
α-myc (Chk1)
63
(kDa)
F
H1299
IP: IgG α-Chk1
Nutlin-3a (μM) 0 0 5 10
IP
α-PGAM
28
α-Chk1
48
Total lysate
α-PGAM
28
α-Chk1
48 (kDa)
H
p53-/- MEFs
Total lysate
Ni-NTA bound
PGAM1-FLAG WT WT W68A W78A WT WT W68A W78A
Chk1-myc-his - + + + - + + +
α-FLAG (PGAM)
36
α-myc (Chk1)
63
(kDa)
I
p53-/- MEFs
Total lysate
Ni-NTA bound
PGAM1-FLAG WT WT W68A W78A WT WT W68A W78A
Chk1-myc-his - + + + - + + +
Ras-G12V + + + + + + + +
α-FLAG (PGAM)
36
α-myc (Chk1)
63
(kDa)
J
p53-/- MEFs
Total lysate
Ni-NTA bound
PGAM2-FLAG WT WT W68A W78A WT WT W68A W78A WT WT W68A W78A WT WT W68A W78A
Chk1-myc-his - + + + - + + + - + + + - + + +
Ras-G12V - - - - + + + + - - - - + + + +
α-FLAG (PGAM)
36
α-myc (Chk1)
63
(kDa)
G
PGAM1-FLAG
- WT W68A W78A
α-FLAG (PGAM)
36
α-Actin
48
(kDa)
Relative PGAM activity
Vector WT W68A W78A
K
PGAM2
p53-/- MEFs + Chk1 vector WT W68A W78A
Relative value of mRNA
Hk1 Gpi Pfkl Aldoa Tpi Gapdh Pgk1 Pgam1 Eno1
L
p53-/- MEFs
Ras-G12V + Chk1
Vector
Ras-G12V
Relative cell number
Vector WT W68A W78A
PGAM2

Figure S8. Nutlin and binding-deficient mutations in PGAM interfere with the interaction between PGAM and Chk1, but not with PGAM enzymatic activity. Related to Figure 5, 6 and 7

(A) The impact of AKT inhibition against PGAM-Chk1 interaction. H1299 cells were treated with Triciribine. Immunoprecipitation assay were performed using anti-Chk1 antibody. Ser473 phosphorylation on AKT was evaluated. **(B)** The interaction between p53 and Mdm2 during Nutlin-3a treatment was evaluated by immunoprecipitation assay. *p53*$^{-/-}$ MEFs expressing the indicated vectors were exposed to 5 μM or 10 μM Nutlin-3a for 48 h, followed by treatment with 20 μM MG132 for 3 h. The lysates were immunoprecipitated with anti-p53 antibody. **(C)** Enzymatic activity of recombinant PGAM1 and 2 proteins was assessed in the presence of Nutlin-3a. Various amounts of recombinant PGAM1 and 2 proteins (2.5, 5, 10, and 20 ng) were incubated with indicated concentrations of Nutlin-3a (upper and lower panel, respectively). Data represent the mean ± SEM. **(D)** The effect of Nutlin-3a on PGAM1 and Mdm2 interaction was evaluated by the immunoprecipitation assay. **(E)** The evaluation of PGAM1 and Chk1 interaction under Nutlin-3a treatment by the immunoprecipitation assay. **(F)** The effect of Nutlin-3a on endogenous PGAM-Chk1 binding in H1299 cells. Cells were exposed to Nutlin-3a for 48 h. After treatment with 20 μM MG132 for 3 h, the immunoprecipitation assay was performed, using the indicated antibodies. **(G)** PGAM enzymatic activity in Chk1-expressing *p53*$^{-/-}$ MEFs retrovirally infected with the indicated vectors (empty vector, PGAM1-WT-FLAG, PGAM1-W68A-FLAG, and PGAM1-W78A-FLAG) (*n* = 3 each; right panel). Protein levels for various versions of PGAM1-FLAG were shown by western blotting (left panels). **(H and I)** His-tagged protein pulldown assay. The Chk1-binding activity of PGAM1 mutants (W68A and W78A) compared to that of PGAM1-WT was analyzed in the absence or presence of oncogenic Ras (H and I, respectively). **(J)** The interaction of PGAM2-W68A or -W78A mutant with Chk1. The Chk1-binding activity in various versions of PGAM2 (WT, W68A, or W78A) was assessed by His-tagged protein pulldown assay in the presence or absence of Ras-G12V. Chk1-expressing *p53*$^{-/-}$ MEFs with indicated genes were analyzed. **(K)** Comparison of mRNA levels for glycolytic enzymes in indicated Chk1-expressing *p53*$^{-/-}$ MEFs with PGAM2 variants (WT, W68A, or W78A) (*n* = 3). The data are relative to expression in control cells with the empty vector. **(L)** Comparison of cell proliferation *in vitro*. The effect of PGAM2 variants (WT, W68A, or W78A) on cell growth was assessed by crystal violet staining in Chk1-expressing

p53$^{-/-}$ MEFs with or without Ras-G12V as shown in Figure 7F. The staining intensities for three independent assays were shown as relative cell numbers against control. **$P < 0.005$, Dunnett's multiple comparison test. Data represent the mean ± SEM.

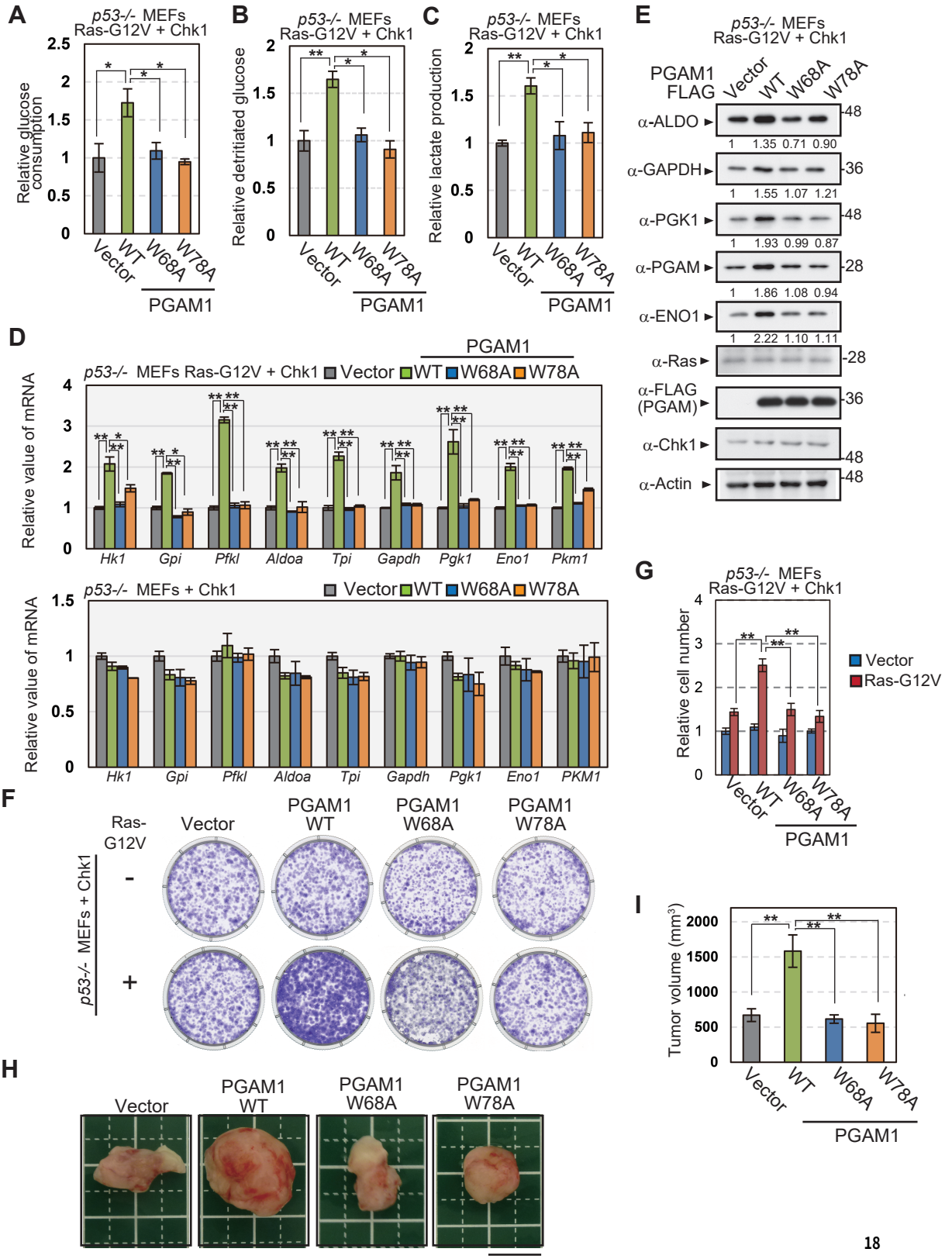
A
p53-/- MEFs
Ras-G12V + Chk1
Relative glucose consumption
Vector
WT
W68A
W78A
PGAM1
B
Relative detriated glucose
C
Relative lactate production
D
Relative value of mRNA
Hk1
Gpi
Pfkl
Aldoa
Tpi
Gapdh
Pgk1
Eno1
Pkm1
p53-/- MEFs + Chk1
PKM1
E
PGAM1 FLAG
α-ALDO
α-GAPDH
α-PGK1
α-PGAM
α-ENO1
α-Ras
α-FLAG (PGAM)
α-Chk1
α-Actin
1 1.35 0.71 0.90
1 1.55 1.07 1.21
1 1.93 0.99 0.87
1 1.86 1.08 0.94
1 2.22 1.10 1.11
G
Relative cell number
Vector
Ras-G12V
F
Ras-G12V
PGAM1 WT
PGAM1 W68A
PGAM1 W78A
H
I
Tumor volume (mm3)

Figure S9. PGAM1 mutants with W68A or W78A abolished the enhancement of glycolysis and proliferation in oncogenic Ras expressing cells. Related to Figure 7

(A-E) Comparison of glycolytic profiles among the cells expressing PGAM1 variants (WT, W68A, or W78A) in the presence of Ras-G12V. Glucose consumption **(A)**, glucose flux **(B)**, and lactate production **(C)** were analyzed among indicated cells on the common genetic background of *p53*$^{-/-}$ with Ras-G12V and Chk1 (n = 3). The mRNA and protein levels of glycolytic enzymes were also evaluated in indicated cells **(D and E)**. **(F and G)** The effect of indicated PGAM1 variants on cell growth *in vitro*. Crystal-violet staining was assessed in Chk1-expressing *p53*$^{-/-}$ MEFs with or without Ras-G12V **(F)**. Intensities of crystal-violet staining were measured **(G)**. **(H and I)** *in vivo* tumor growth assay in nude mice. *p53*$^{-/-}$ MEFs, expressing Ras-G12V, Chk1, and the indicated versions of PGAM1, were injected subcutaneously into nude mice (n=6). **(H)** Representative images of tumors. **(I)** Measurement of tumor volumes are shown. **P* < 0.05 and **P < 0.005, Dunnett's multiple comparison test. Data represent the mean ± SEM.

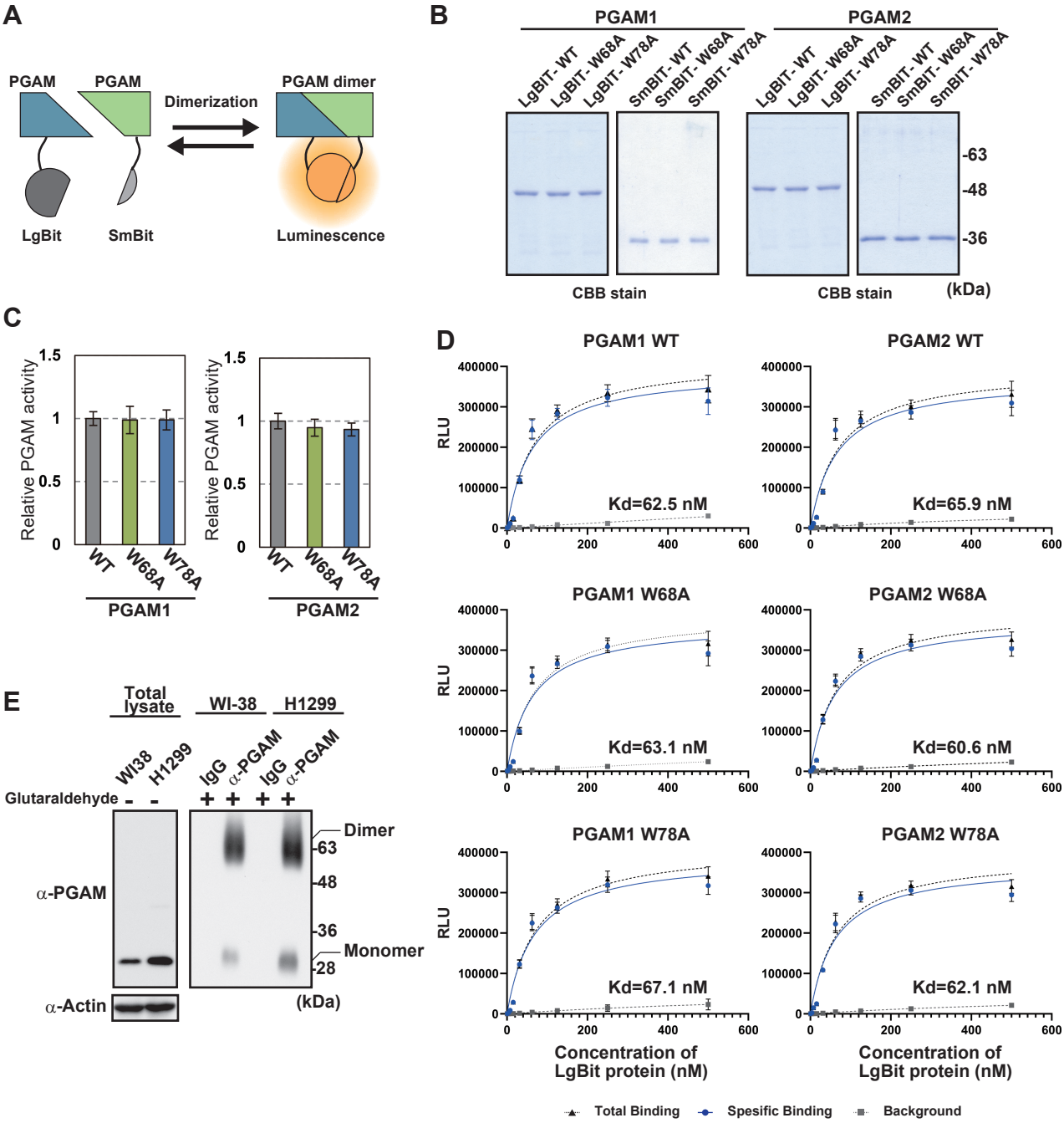
A
PGAM
PGAM
Dimerization
PGAM dimer
LgBit
SmBit
Luminescence
B
PGAM1
PGAM2
LgBIT- WT
LgBIT- W68A
LgBIT- W78A
SmBIT- WT
SmBIT- W68A
SmBIT- W78A
-63
-48
-36
CBB stain
CBB stain
(kDa)
C
Relative PGAM activity
1.5
1
0.5
0
WT
W68A
W78A
PGAM1
PGAM2
D
PGAM1 WT
PGAM2 WT
PGAM1 W68A
PGAM2 W68A
PGAM1 W78A
PGAM2 W78A
RLU
Kd=62.5 nM
Kd=65.9 nM
Kd=63.1 nM
Kd=60.6 nM
Kd=67.1 nM
Kd=62.1 nM
Concentration of LgBit protein (nM)
Total Binding
Spesific Binding
Background
E
Total lysate
WI-38
H1299
WI38
H1299
IgG
α-PGAM
Glutaraldehyde
α-PGAM
α-Actin
Dimer
Monomer
(kDa)

Figure S10. The dimerization efficiency in various versions of PGAM1 and PGAM2. Related to Figure 7

(A) Schematic diagrams of NanoBiT systems. Dimerization of PGAM proteins with large and small NanoBiT tag produces luminescence. **(B)** Coomassie Brilliant Blue staining for indicated recombinant proteins prepared from bacteria. **(C)** Measurement of PGAM enzymatic activity in indicated LgBiT-tagged PGAM recombinant proteins. **(D)** Saturated binding of SmBiT-PGAM to LgBiT-PGAM was assessed. 0.25 nM SmBiT-PGAM proteins were incubated with various concentration of indicated LgBiT-PGAM proteins. NanoBiT luminescence of dimerized PGAM proteins was measured. The left panels show dimerization of PGAM1 WT (top), PGAM1 W68A (middle), PGAM1 W78A (bottom), while the right panels indicate those of PGAM2 WT (top), PGAM2 W68A (middle) and PGAM2 W78A (bottom). Triangle; total binding curve of the complex between LgBiT and SmBit proteins. Square; background curve of LgBiT proteins only. Specific binding curve (circle) is obtained by subtracting background signals from total binding ones. Binding dissociation constant (Kd) was estimated from the curve of specific binding. **(E)** Evaluation of monomer and dimer forms of PGAM in H1299 and WI-38 cells. After 100kd cutoff filtration, the protein extracts from indicated cells were immunoprecipitated by anti-PGAM1 antibody. After the elution of PGAM protein from PGAM1 antibody-conjugated beads by specific peptides, eluted proteins were cross-linked by 0.5% glutaraldehyde for 5 min. Immunoblotting detected monomer or dimer of PGAM proteins (right panel). Left panels showed the immunoblotting in total cell lysates of indicated cells without cross-link.

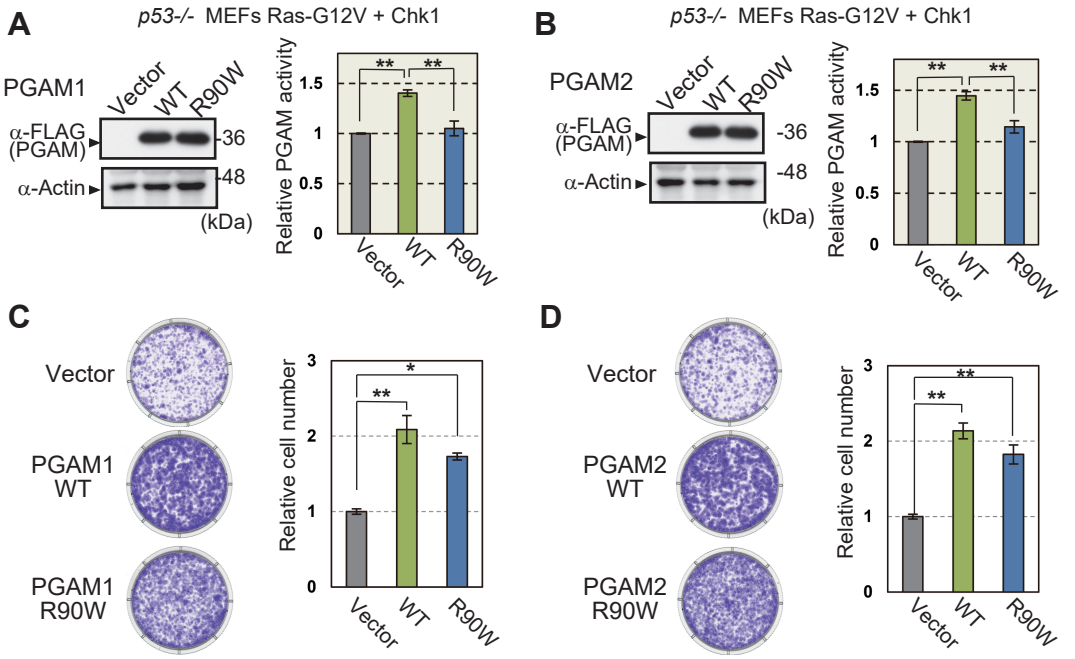
A
p53-/- MEFs Ras-G12V + Chk1
PGAM1
Vector
WT
R90W
α-FLAG (PGAM)
α-Actin
-36
-48
(kDa)
Relative PGAM activity
1.5
1
0.5
0
**
**
Vector
WT
R90W
B
p53-/- MEFs Ras-G12V + Chk1
PGAM2
Vector
WT
R90W
α-FLAG (PGAM)
α-Actin
-36
-48
(kDa)
Relative PGAM activity
1.5
1
0.5
0
**
**
Vector
WT
R90W
C
Vector
PGAM1 WT
PGAM1 R90W
Relative cell number
3
2
1
0
*
**
Vector
WT
R90W
D
Vector
PGAM2 WT
PGAM2 R90W
Relative cell number
3
2
1
0
**
**
Vector
WT
R90W

Figure S11. The impact of enzymatic mutant PGAM-R90W on cell growth. Related to Figure 7

(A and B) Enzymatic mutation *R90W* was introduced in PGAM1 (A) and PGAM2 (B). Western blotting was performed to detect FLAG tagged PGAM proteins (left panels). PGAM enzymatic activities were measured in indicated cells (right panels). **(C and D)** Crystal-violet (CV) staining was assessed in indicated cells to evaluate their proliferative capacity (left panels). The intensities of CV staining were evaluated (right panels).

Table S1. The list of cancer-related genetic aberrations

	H1299	HSC-1	HSC-5	Hs578T	MDA-MB-231	BT-474	HCT116	RKO	SW480	DLD-1	HT-29	SJSA-1	U2OS	Hek293	HepG2
ABL1		*[1]	*[1]	*K7R*			*Y257C*	*F747I*						*[1]	
AKT1		*[1]	*[1]											*[1]	
ALK		*[1]	*[1]											*[1]	
APC		*[1]	*[1]					*K1454E*	*Q1338**	*I1417fs*2 K993N R727M*	*E853* T1556fs**			*[1]	
ATM		*[1]	*[1]		*N1005I*	*E2468K*	*A1127V*		*R2461P*					*[1]	*V2906I*
BRAF		*[1]	*[1]		*G464V*			*V600E*			*V600E T119S*			*[1]	
CDH1		*[1]	*[1]				*H121fs*94*							*[1]	
CDKN2A		*[1]		*c.1_471 de*	*c.1_471 de*		*R24fs*20 E74fs*15*							*[1]	
CSF1R		*[1]	*[1]											*[1]	
CTNNB1		*[1]	*[1]				*S45del*							*[1]	*W25_I140de*
EGFR		*amp*[2]			*L469W*									*[1]	
ERBB2		*[1]	*[1]					*L796P*						*[1]	
ERBB4		*[1]	*[1]											*[1]	
EZH2		*[1]	*[1]					*E169K*		*R418Q*				*[1]	
FBXW7		*[1]	*[1]											*[1]	
FGFR1		*[1]	*[1]				*A343V*	*P150L*		*A268S*				*[1]	
FGFR2		*[1]	*[1]				*P582L*							*[1]	
FGFR3		*[1]	*[1]											*[1]	
FLT3		*[1]	*[1]				*V197A P986fs*>8*							*[1]	
GNA11		*[1]	*[1]											*[1]	
GNAS		*[1]	*[1]				*Y316C*			*K338N*				*[1]	
GNAQ		*[1]	*[1]				*A102G*							*[1]	
HNF1A		*[1]	*[1]	*K273E*		*Q495**	*P174fs*51*	*P379fs*5*						*[1]	
HRAS		*[1]	*[1]	*G12D*										*[1]	
IDH1		*[1]	*[1]				*S261L*			*G97D*				*[1]	

Table S1. The list of cancer-related genetic aberrations (continued)

	H1299	HSC-1	HSC-5	Hs578T	MDA-MB-231	BT-474	HCT116	RKO	SW480	DLD-1	HT-29	SJSA-1	U2OS	Hek293	HepG2
IDH2		*1	*1					*G190D*						*1	
JAK2		*1	*1											*1	
JAK3		*1	*1											*1	
KDR		*1	*1											*1	
KIT		*1	*1							*R135H*				*1	
KRAS		*1	*1		*G13D*		*G13D*		*G12V*	*G13D*		*Q61H*		*1	
MET		*1	*1				*L238fs*25*							*1	
MLH1		*1	*1				*S252**	*L323M*		*A120S*				*1	
MPL		*1	*1											*1	
NOTCH1		*1	*1				*P915L G1195R*	*Q2343R*						*1	
NPM1		*1	*1											*1	
NRAS	*Q61K*	*1	*1									*Q61K*		*1	*Q61L*
PDGFRA		*1	*1		*Y172F*									*1	
PIK3CA		*1				*K111N*	*H1047R*	*H1047R*		*D549N E545K*	*P449T*			*1	
PTEN		*1												*1	
PTPN11		*1	*1											*1	
RB1		*1	*1											*1	
RET		*1	*1											*1	
SMAD4		*1	*1								*Q311**			*1	
SMARCB1		*1	*1											*1	
SMO		*1	*1				*V404M*			*T640A*				*1	
SRC		*1	*1											*1	
STK11		*1	*1											*1	
TP53	*del*	*V173L*	*1	*V157F*	*R280K*	*E285K*			*P309S R273H*	*S241F*	*R273H*	*Mdm2 amp*2*		*1	
VHL		*1	*1												

Table S1. List of cancer-related mutations in 15 cancer cell lines. Related to Figure 5

Summary of identified mutations in 15 cancer cell lines. These cells were tested in Figure 5B and S7B. Fifty cancer-related genes were proposed by Tsongalis et al (Tsongalis et al., 2014).

Gene mutations in 15 cancer cells were described in the following literatures (Cancer Genome Atlas Research, 2008; Fujii et al., 1995; Hori et al., 2009; Klijn et al., 2015; Oliner et al., 1992).

*[1] Not determined,

*[2] amp stands for amplification,

Table S2 Genetic aberrations of lung adenocarcinoma cell lines

Cells having genetic aberrations either in p53 or Ras pathway

	Genetic aberrations				
	EGFR	***KRAS***	***NRAS***	***HRAS***	***p53***
A427		*G12D*			
A549		*G12S*			
H1437					*R267P*
H1648					*L35Fs*8*
H1703					*c919+1G>T*
H1819					*c933+1G>T*
H2126					*E62**
H2228					*Q331**
H2347		*L19F* *R481H*	*Q61R*		
H322					*Arg248Leu*
PC-3					*K139fs*31*
RERF-LC-KJ					*E224D*
VMRC-LCD					*R175H*
LC2					*S241C*

Table S2. Genetic aberrations of lung adenocarcinoma cell lines (continued)

Cells having genetic aberrations both in p53 and Ras pathways

	Genetic aberrations				
	EGFR	***KRAS***	***NRAS***	***HRAS***	***p53***
ABC-1	*L858R*				*P278S*
H1299			*Q61K*		*c1_954>AAG*
H1650	*E746_A750del*				*c673-2A>G*
H1975	*T790M, L858R*				*R273H*
II-18	*L858R*				*K164**
PC-14	*E746_A750del*				*Arg248Trp*
PC-7	*G719S*	*G12V*			*His214Arg*
PC-9	*E746_A750del L858R*				*Arg248Gln*
RERF-LC-MS		*K12S*			*F134fs*14*
RERF-LC-OK	*L858R*				*F113C*
RERF-LC-ad1		*G12A*			*P278F*
RERF-LC-ad2	*L747_A750>P*				*A159V*

Table S2. Classification of 26 non-small cell lung cancer (NSCLC) cell lines. Related to Figure 5

26 NSCLC cell lines were classified into two subgroups according to gene aberrations of *p53* and *Ras* pathways.

Upper list shows 14 cells harboring genetic aberrations either in p53 or Ras pathway, while lower list indicates 12 cells with genetic aberrations in both pathways.

Gene mutations of NSCLC cells were described in the following literatures (Barretina et al., 2012; Chen et al., 1993; Fujita et al., 1999; Iwakawa et al., 2010; Kashii et al., 1994; Kaufman et al., 2017; Nagai et al., 2005; Notsuda et al., 2013; Wei et al., 2003)

Table S3. The primer sequences for real-time qRT-PCR

Name	Sequence
mouse *Rpl13a* qRT Fw	5’- TGC TGC TCT CAA GGT TGT TCG -3’
mouse *Rpl13a* qRT Re	5’- GCC TTT TCC TTC CGT TTC TCC -3’
mouse *Hk1* qRT Fw	5'-AAG AAT GGC CTC TCC CGG-3
mouse *Hk1* qRT Re	5'-CGC CGA GAT CCA GTG CAA TG-3'
mouse *Hk2* qRT Fw	5'-ATA TGG TTG CCT CAT CTT GG-3'
mouse *Hk2* qRT Re	5'-CTC CCT CCC TCC CAA TG-3'
mouse *Hk3* qRT Fw	5'-ATT CCT GGA TGC ATA CCC CGT -3'
mouse *Hk3* qRT Re	5'-GCC GCT GCA CCT AAA ACC TTT -3'
mouse *Gpi* qRT Fw	5'-CCA ATG CAG AGA CAG CAA AGG-3'
mouse *Gpi* qRT Re	5'-CACTTTGGCCGTGTTCGTAGA-3'
mouse *Pfkm* qRT Fw	5'-TGG AGC GAC TTG CTG AAT GAT -3'
mouse *Pfkm* qRT Re	5'-TCA TTG TCG ATT GAG CCA ACC -3'
mouse *Pfkl* qRT Fw	5'-GCT GCA ATG GAG TTG TG-3'
mouse *Pfkl* qRT Re	5'-GTA GCC AGG TAGC CAC AG-3'
mouse *Tpi* qRT Fw	5'-TGC CAA ACA ATG AGC ACT GC-3'
mouse *Tpi* qRT Re	5'-ATC AGA AGC ATG TGA CCG GTG-3'
mouse *Aldoa* qRT Fw	5'-CTG GCC ATC ATG GAA AAT GC-3'
mouse *Aldoa* qRT Re	5'-TCA AGT CAT GGT CCC CAT CAG-3'
mouse *Aldob* qRT Fw	5'-ATC GGC GGA GTG ATC CTT TT-3'
mouse *Aldob* qRT Re	5'-TCC AAC TTG ATG CCC ACC A -3'
mouse *Gapdh* qRT Fw	5'-AGC CTC GTC CCG TAG ACA AAA-3'
mouse *Gapdh* qRT Re	5'-TGG CAA CAA TCT CCA CTT TGC-3'
mouse *Pgk1* qRT Fw	5'-TTT GGA CAA GCT GGA CGT GAA-3'
mouse *Pgk1* qRT Re	5'-GCT TGG AAC AGC AGC CTT GAT-3'
mouse *Pgam1* qRT Fw	5'-GTT GCG AGA TGC TGG CTA TGA-3'
mouse *Pgam1* qRT Re	5'-CAC ATC TGG TCA ATG GCA TCC-3'
mouse *Pgam2* qRT Fw	5’-TGG AAT GAG GAG ATC GCA CCT -3’
mouse *Pgam2* qRT Re	5’-TCG GAC ATC CCT TCC AGA TGT -3’
mouse *Eno1* qRT Fw	5'-TAT TGC GCC TGC TCT GGT TAG-3'
mouse *Eno1* qRT Re	5'-GGA TGG CAT TTG CAC CAA AT-3'
mouse *Eno3* qRT Fw	5'-GGA GAA GAA GGC CTG CAA TTG -3'
mouse *Eno3* qRT Re	5'-CCC AGC CAT TAG ATT GTG CAA -3
mouse *Pkm1* qRT Fw	5'-CTG TTT GAA GAG CTT GTG GCG -3
mouse *Pkm1* qRT Re	5'-CTG CTA AAC ACT TAT AAG AGG CC -3
mouse *p16INK4* qRT Fw	5'-CCC AAC GCC CCG AAC T -3'
mouse *p16INK4* qRT Re	5'-GCA GAA GAG CTG CTA CGT GAA -3

Table S3. Primers for real-time qRT-PCR (continued)

Name	Sequence
mouse *p21CIP1* qRT Fw	5'-AGA CAT TCA GAG CCA CAG GCA-3'
mouse *p21CIP1* qRT Re	5'- ATG AGC GCA TCGCAA TCA C -3
mouse *Bax* qRT Fw	5'-AGC AAA CTG GTG CTC AAG G -3'
mouse *Bax* qRT Re	5'-AGA CAA GCA GCC GCT CAC -3
mouse *Fas* qRT Fw	5'-CAG ACA TGC TGTGGA TCT GG -3'
mouse *Fas* qRT Re	5'-CCT CAG CTT TAA ACT CTC GGA -3
human *Rpl13a* qRT Fw	5'-CTG GAC CGT CTC AAG GTG TT -3'
human *Rpl13a* qRT Re	5'-GCC CCA GAT AGG CAA ACT T -3'
human *Hk1* qRT Fw	5'-ACA TTG TCT CCT GCA TCT CTG -3'
human *Hk1* qRT Re	5'-GCC TTA AAA CCC TTT GTC CAC -3'
human *Gpi* qRT Fw	5'-GCT TCT ACC AAT GGG CTC ATC -3'
human *Gpi* qRT Re	5'-TGT CCA GGA ACA TGC AGT G -3'
human *Pfkl* qRT Fw	5'-AAC GAG AAG TGC CAT GAC TAC -3'
human *Pfkl* qRT Re	5'-GTC CCA TAG TTC CGG TCA AAG -3'
human *Tpi* qRT Fw	5'-TCA TCG CAG ATA ACG TGA AGG -3'
human *Tpi* qRT Re	5'-CAT CAG AGA CGT TGG ACT TCA G -3'
human *Aldoa* qRT Fw	5'- GGT GTC ATC CTC TTC CAT GAG -3'
human *Aldoa* qRT Re	5'-GTA GTC TCG CCA TTT GTC CC -3'
human *Gapdh* qRT Fw	5'-CTT TGT CAA GCT CAT TTC CTG G -3'
human *Gapdh* qRT Re	5'-TCT TCC TCT TGT GCT CTT GC -3'
human *Pgk1* qRT Fw	5'- GCT TCT GGG AAC AAG GTT AAA G-3'
human *Pgk1* qRT Re	5'- CTG TGG CAG ATT GAC TCC TAC -3'
human *Pgam1* qRT Fw	5'-GGA GGC GCT CCT ATG ATG TC -3'
human *Pgam1* qRT Re	5'-ATC TTC TGT GAG GTC TGC ATA C -3'
human *Eno1* qRT Fw	5'- TTG GAG CAG AGG TTT ACC AC -3'
human *Eno1* qRT Re	5'- TTC CCA ATA GCA GTC TTC AGC-3'
human *Pkm1* qRT Fw	5'- CCA TAA TCG TCC TCA CCA AGT C-3'
human *Pkm1* qRT Re	5'- GGA AGA TGC CAC GGT ACA -3'
human *Chk1* qRT Fw	5'-GAG AAT CCA TCA GCA AGA ATT ACC -3'
human *Chk1* qRT Re	5'-GAA TGT GCT TAG AAA ATC CAC TGG-3'
human *Hif1* qRT Fw	5'-AAC ATA AAG TCT GCA ACA TGG AAG -3'
human *Hlf1* qRT Re	5'-TTT GAT GGG TGA GGA ATG GG -3'

Table S3. Primers for real-time qRT-PCR. Related to Figure 1 to 7
Sequences of primer used for real-time qRT-PCR in this study.

Transparent Methods

Cell culture

The human cell lines H1299, RKO, SW480, DLD-1, HT-29, Hs578t, MDA-MB-231, BT-474, U2OS, and SJSA-1 were obtained from American Type Culture Collection, and HCT116, Hek293, HepG2, and WI-38 were from RIKEN Bioresources Center. HSC-1 and HSC-5 were obtained from the Japanese Collection of Research Bioresources. The PLAT-A packaging cell line was a kind gift from Dr. Toshio Kitamura (University of Tokyo). The human cell lines (H1299, Hs578t, MDA-MB-231, BT-474, HCT116, RKO, SW480, DLD-1, HT-29, HEK293, HepG2, SJSA-1, U2OS, and WI-38) were cultured in Dulbecco's modified Eagle medium (DMEM) containing 10% fetal bovine serum (FBS). HSC-1 cells were cultured in DMEM with 20% FBS. HSC-5 cells were cultured in Iscove's modified Dulbecco's medium with 10% FBS. MEFs isolated from embryos (postcoital day 13.5) of C57BL/6 mice were grown in DMEM with 10% FBS and antibiotics (Carnero et al., 2000). *Pgam1*$^{flox/flox}$ *ER-Cre* MEFs were generated by crossing between *CAG-ER-Cre* mice (Hayashi and McMahon, 2002) and *Pgam1*$^{flox/flox}$ mice. At passage 4, *Pgam1*$^{flox/flox}$ *ER-Cre* MEFs or *Pgam1*$^{flox/fox}$ MEFs were treated with 0.5 μM 4-OHT for 4 days. Ablation of PGAM was detected by immunoblotting. All cell lines were tested and shown to be negative for mycoplasma contamination.

Cytochemical staining for SA-β-Gal was performed (Dimri et al., 1995). At passage 6 and 10, *Pgam1*$^{flox/flox}$ *ER-Cre* or *Pgam1*$^{flox/flox}$ MEFs were washed twice with ice-cold phosphate-buffered saline (PBS) buffer and were treated by fixation solution (2% formaldehyde and 0.2 % glutaraldehyde in PBS buffer) for 5 min at room temperature. After removing the fixation solution, cells were washed twice with PBS buffer and were incubated with staining solution (40 mM citric acid /Na phosphate buffer, 5 mM $K_4[Fe(CN)6]$ $3H_2O$, 5 mM $K_3[Fe(CN)_6]$, 150 mM NaCl, 2 mM $MgCl_2$, 1 mg/ml X-gal) for overnight at 37°C. Images were recorded using a microscope (IX-73, Olympus, Tokyo, Japan),

Cells were subjected to retroviral infection or transfection of plasmids. For the proliferation assay, 5×10^3 cells were plated on 6-cm dishes. After 10 days of culture, cells were fixed with 2% glutaraldehyde, followed by crystal violet staining. Then the staining was resolved by 1% sodium dodecyl sulfate. The optical density was determined at 590 nm.

Plasmid DNA

Expression of full-length mouse *Pgam1* and *Pgam2* with a C-terminal 3X FLAG tag and deletion mutants of *Pgam2* (TN, T4, and TC) with a C-terminal 3X FLAG tag driven by the CMV promoter of the p3xFLAG-CMV14 expression vector were constructed previously (Mikawa et al., 2014). The deletion mutants of *Pgam1* (TN, T4, and TC) with a C-terminal 3X FLAG tag were generated by PCR. The relevant variants of *Pgam1* and *Pgam2* mutamts *(W68A*, *W78A and R90W*) were generated

by PCR-based mutagenesis. pHygro MarxIV retroviral vectors encoding mouse *Pgam1* and *Pgam2* variants were also generated. The relevant variant *Pgam1* and *Pgam2* cDNAs were ligated into the XhoI site of Hygro Marx IV vectors. The pBabe-puro-Ras-G12V plasmid was a gift from Dr. Kayoko Maehara (Kio University, Nara, Japan). The pcDNA3.1 Chk1-myc-his vector was previously described (Niida et al., 2007). *Chk1* cDNAs were sub-cloned into WZLneo retroviral vectors. Human *p53* cDNA was sub-cloned into the pcDNA3.1 vector containing a 3X HA sequence between the NheI and XhoI sites. Expression of full-length p53 with an N-terminal 3X HA-tag was driven by the CMV promoter. Expression vector of human Mdm2 with an N-terminal HA-tag was constructed previously (Mikawa et al., 2014). NanoBiT vectors were generated using Flexi Vector Systems (Promega). In brief, wild type and relevant mutants of *Pgam1* and *Pgam2 (W68A*, *W78A*) were subcloned into pF4A plasmid. Subsequently, those relevant variants of Pgam were subcloned into N-terminus LgBiT-tagging plasmid (pFN33K) or SmBiT-tagging plasmid (pFN35K).

Reagents

Reagents were obtained as follows. UCN01, DMBA, TPA, and Nutlin-3a from Sigma–Aldrich (St. Louis, MO). MG132 from Peptide Institute, Inc. (Osaka, Japan). U126 and Triciribine from FUJIFILM Wako Pure Chemical Corporation (Osaka, Japan). BI D-1870 from Selleck (Houston, TX).

Mouse models

All procedures for animal experiments were performed in accordance with the principles and guidelines of the Animal Care and Use Committees of Kyoto University Graduate School of Medicine.

Pgam2-Tg mice were generated previously (Mikawa et al., 2014). *Pgam2-Tg* is a strain of transgenic C57BL/6 mice that overexpresses the *Pgam2* with a 3xFLAG tag under the cytomegalovirus immediate-to-early enhancer element and chicken *β-actin* promoter (*CAG*) (Niwa et al., 1991) For generation of the *Pgam1* KO mouse, the targeting vector was constructed as follows. Exons 2–4 of mouse *Pgam1* were flanked by two loxP sequences, and a FLP recognition target (*FRT*)-flanked neo-cassette was inserted upstream of exon 2. The targeting vector was introduced into mouse embryonic stem cells (C57BL/6), which were injected into blastocysts (BALB/c). Generated founder mice ($Pgam1^{flox/+}$ [neo+]) were crossed with *FLP* transgenic mice for removal of the neo-cassette from heterozygous *flox* mice. $Pgam1^{+/-}$ mice were generated by crossing $Pgam1^{flox/+}$ mice and *CAG-Cre* Tg mice, which ubiquitously express Cre recombinase under the *CAG* promoter. Genotyping was performed using PCR.

Mouse experiments

For assessment of inflammatory response, control or *Pgam2-Tg* mice (18 weeks old, male) were treated with 10 ng TPA on the ears, and the thickness of the ears was measured by constant pressure thickness gauge (PG-201, TECLOCK, Japan).

Chemically induced skin tumorigenesis was performed (Takeuchi et al., 2010). Briefly, seven age-matched (12–15 weeks old, male) pairs of control or *Pgam2-Tg* mice were shaved and treated with 100 μg DMBA in 100 μl acetone. Mice were subsequently treated twice weekly with 12.5 μg TPA in 100 μl acetone for 20 weeks. The number and size of papillomas per mouse were recorded every 2 weeks. The nude mouse xenograft assay was performed (Mikawa et al., 2014). *CAnN.Cg-Foxn^{nu}/CrlCrlj* mice (8 weeks old, male) were injected subcutaneously with 5 × 10^6 cells suspended in 100 μl phosphate-buffered saline. Tumor formation was assessed after 2 weeks.

Transfection and retroviral infection

Transfection of siRNA for mouse *Pgam1*, human *Pgam1* (Life Technologies, Carlsbad, CA), and human *Chk1* (Sigma–Aldrich, St. Louis, MO) was performed using Lipofectamine siRNA MAX (Invitrogen, Carlsbad, CA). Expression vectors were transfected by polyethylenimine MAX (Polysciences, Warrington, PA). The PLAT-A packaging cell line was used for retroviral production (Morita et al., 2000). Retrovirus-infected cells were treated with hygromycin (75 μg/mL), G418 (400 μg/mL), or puromycin (2 μg/mL) for positive selection of infected cells.

Immunoblotting and immunoprecipitation

For immunoblotting, cell lysates were prepared (Carnero *et al.*, 2000). Cells were washed twice with ice-cold PBS and lysed in buffer containing 50 mM Tris–HCl (pH 7.5), 200 mM NaCl, 1 mM ethylenediaminetetraacetic acid (EDTA), 10% glycerol, 0.5% Triton-X100, 50 mM NaF, 1 mM dithiothreitol (DTT), 1 mM Na_3VO_4, 1 mM phenylmethanesulfonyl fluoride (PMSF), and protease inhibitor cocktail (Sigma–Aldrich). After 30 min on ice, lysates were cleared by centrifugation. Equivalent amounts of protein were resolved by sodium dodecyl sulfate-polyacrylamide gel electrophoresis (SDS-PAGE). Anti-PGAM antibody (1:1000), which recognizes both PGAM1 and PGAM2 (Mikawa *et al.*, 2014). Anti-FLAG (F1804, 1:1000), anti-human Chk1 (C9358, 1:3000), and anti-Actin (A4700, 1:1000) from Sigma–Aldrich. Anti-$p21^{CIP1}$ (ab7960, 1:500), anti-phospho-p53 (Ser23; ab59206, 1:500), anti-Chk2 (ab8108, 1:1000), anti-Aldolase (ab169544, 1:1000), anti-PGK1 (ab38007, 1:1000), anti-ENO1 (ab155102, 1: 1000), anti-PGAM1 (ab129191, 1:1000) and anti-PGAM2 (ab183027, 1:1000) from Abcam (Cambridge, UK). Anti-c-myc (9E10, 1: 200), anti-

human p53 (DO-1, 1:1000), anti-mouse Chk1 (Sc-8404, 1:1000) and anti-Mdm2 (SMP-14, 1:200) from Santa Cruz Biotechnology (Dallas, TX). Anti-mouse p53 (1C12; #2524, 1:1000), anti-phospho-p53 (Ser20; #9287, 1:200), anti-phospho-p53 (Ser15; #9284, 1:1000), anti-phospho-Chk1 (Ser345; #2341, 1:1000), and anti-phospho-Chk2 (Thr68; #2661, 1:500), anti-ERK1/2 (#4370, 1:2000), anti-phospho-ERK1/2 (Thr202/Tyr204, #4370, 1:2000), anti-Bad (#9339, 1:1000), anti-phospho-Bad (Ser112, #9391, 1:500), anti-Akt(pan) (#4691, 1:1000) and anti-phospho-Akt (Ser473, #9271, 1:1000) from Cell Signaling Technology (Danvers, MA). Anti-GAPDH (MAB374, 1:3000) from Merck Milipore (Burlington, MA).

For immunoprecipitation assays, cell lysates were precipitated with the relevant antibody for 2 h. Immune complexes were recovered with protein G-agarose beads, washed four times with lysis buffer, and boiled in 2× Laemmli sample buffer for 5 min. Denatured immune complexes were resolved by SDS-PAGE. The quantification of the immunoblot bands were performed using ImageJ.

Dimer and monomer forms of proteins were detected by the modification of the previous protocol as follows (Jagemann et al., 2008). Cultured cells were lysed with lysis buffer (50 mM Tris–HCl (pH 7.5), 150 mM NaCl, 1 mM EDTA, 10% glycerol, 0.5% Triton-X100, 50 mM NaF, 1 mM Na_3VO_4, 1 mM PMSF and protease inhibitor cocktail (Sigma–Aldrich). After the fractionation by centrifugal 100 kDa cutoff filter (Amicon Ultra-4, Merck Milipore Ltd) for 45 min, the resulting extracts were immunoprecipitated by anti-PGAM1 antibody (ab2220, Abcam) for 2 hours. Immunoprecipitants were incubated with 100 μg/ml synthetic peptide (KAMEAVAAQGKAKK), whose sequence matched with those in C-terminus of PGAM1 protein, the antigenic determinant of anti-PGAM1 antibody. Eluted PGAM proteins were cross-linked by 0.5% glutaraldehyde for 5 min at 37°C. Forms of PGAM proteins were evaluated by immunoblotting.

Measurement of glycolytic enzyme activity

Enzymatic activity of aldolase, GAPDH, PGK and enolase were measured spectrophotometrically using enzyme activity assay kit (BioVision, Milpitas, CA). PGAM enzymatic activity was measured (Kondoh et al., 2005). Briefly, cell lysates or recombinant proteins were incubated in reaction buffer (100 mM Tris–HCl [pH 8.0], 100 mM KCl, 0.5 mM EDTA, 2 mM $MgCl_2$, 0.2 mM NADH, 3 mM ADP, and 10 μM 2,3-diphosphoglycerate) with enzyme mixture (0.6 U lactate dehydrogenase, 0.5 U pyruvate kinase, and 0.1 U enolase). Next, 1mM 3-phosphoglyceric acid was added and incubated at 37°C. Activity was measured as NAD^+ release.

Glycolytic flux measurement

Glycolytic flux was measured (Kondoh et al., 2005). After cells were cultured for 11 h in DMEM containing 25 mM glucose, medium was exchanged for DMEM containing 4.25 mM glucose. After 10 h, D-[3-^{3}H] glucose was added to the medium. After 6 h, an aliquot of medium was precipitated with perchloric acid. The supernatant was applied to a column filled with DOWEX 1X8 200–400 MESH Cl resin (Sigma–Aldrich), and the amount of [^{3}H] water in the flow through was normalized to protein content. The glucose and lactate concentrations in the culture medium were determined using a glucose or lactate assay kit (BioVision), respectively. The value of glucose consumption or lactate production was normalized to the protein content of the corresponding cell lysate.

RNA analysis

Total RNA was extracted with TRIzol (Invitrogen). cDNA pools were generated using the ReverTra Ace qPCR RT kit (Toyobo, Osaka, Japan). Real-time quantitative PCR was performed using the Thermal Cycler Dice Real-Time system (Takara Bio., Kusatsu, Japan) and Thunderbird SYBR qPCR mix (Toyobo). Gene expression levels were normalized to *Rpl13a* mRNA and presented as values relative to controls. The primers used are shown in Table S3.

***In vitro* phosphatase assay**

Phosphatase activity was determined using a serine/threonine phosphatase assay system (Promega). Phosphopeptides were obtained from Scrum Inc. (Tokyo, Japan). Briefly, 5000 pmol phosphopeptide was preincubated in various pH conditions (pH 6.2, 7.2, 8.2, and 9.2) in phosphatase reaction buffer (50 mM imidazole, 0.2 mM ethylene glycol-bis(β-aminoethyl ether)-N,N,N',N'-tetraacetic acid, 5 mM $MgCl_2$, 0.02% beta-mercaptoethanol, and 0.1 mg/mL bovine serum albumin) for 3 min at 30°C (Dhananjaya and D'Souza, 2011). Recombinant PGAM protein or λPPase was added to the reaction and incubated for 30 min at 30°C. Free phosphate was detected as the absorbance by the complex of molybdate, malachite green, and phosphate, according to the manufacturer's protocol. RRA(pT)VA phosphopeptide is compatible as a substrate for several serine/threonine phosphatases such as protein phosphatases 2A, 2B, and 2C (Donella Deana et al., 1990). For assessment of phosphatase activity against phospho-p53 (Ser15), phospho-p53 (Ser20), and phospho-p53 (Ser15 and Ser20) peptides, 5000 pmol phosphopeptides were incubated with 500 ng recombinant PGAM1 or PGAM2 protein or 250 ng λPPase in phosphatase reaction buffer (pH 7.2). The phospho-p53 peptide sequences were described previously (Shreeram

et al., 2006).

NanoBiT assay

NanoLuc Binary Technology (NanoBiT) assay (Promega) is utilized to quantify protein-protein interaction between the proteins with large and small NanoBiT tag (Dixon et al., 2016). NanoLuc is newly invented smaller luciferase than standard luciferase, but much more stable with production of much brighter luminescence. NanoBiT comprises two complementary small and large subunits (SmBiT and LgBiT, respectively), whose assembly generates luminescence. This technology was applied for accurate measurement of protein interactions (Song et al., 2020). We generated recombinant PGAM1, 2-WT, W68A, and W78A proteins with NanoBiT tags from the extract of bacteria. A saturation assay was performed using low levels (0.25 nM) of SmBiT fusion proteins for the binding with LgBiT partners at increasing concentrations (0.98 to 500 nM). LgBiT fusion proteins were incubated with or without SmBiT fusion protein in binding buffer (1% BSA in PBS) for 60 min. At the end of incubation, binding intensity was measured as luminescent emission by GloMAX navigator (Promega). Specific binding intensity was obtained by subtraction of background signal (luminescence of LgBiT protein only) from total binding signal (luminescence of LgBiT protein with SmBit protein). For estimation of binding dissociation constant (Kd), we used 1:1 binding model and the curve of specific binding was fitted using GraphPad prism 8 (GraphPad software, CA).

Prognosis analysis

The correlation between the expression level of PGAM1 or Chk1 and the survival rates of NSCLC patients was assessed by the minimum P-value approach using the PrognoScan database (Mizuno et al., 2009). Dataset of Jacob-00182-MSK was evaluated (Director's Challenge Consortium for the Molecular Classification of Lung et al., 2008). NSCLC patients were classified into two groups according to PGAM1 or Chk1 expression levels in their tumors at all possible cutoff points. The P-value of risk differences between any two groups were analyzed using the log-rank test. The cutoff was selected at the point giving the most significant P-value.

Statistical analysis

All data are expressed as the mean ± standard error of the mean (SEM) from at least three independent experiments. Comparisons between two independent groups were analyzed using an unpaired Student's two-tailed t-test. Comparisons between multiple groups were analyzed using one-way analysis of variance and Dunnett's multiple comparison test.

Supplemental references

Barretina, J., Caponigro, G., Stransky, N., Venkatesan, K., Margolin, A.A., Kim, S., Wilson, C.J., Lehar, J., Kryukov, G.V., Sonkin, D.*, et al.* (2012). The Cancer Cell Line Encyclopedia enables predictive modelling of anticancer drug sensitivity. Nature *483*, 603-607.

Carnero, A., Hudson, J.D., Price, C.M., and Beach, D.H. (2000). p16INK4A and p19ARF act in overlapping pathways in cellular immortalization. Nature cell biology *2*, 148-155.

Chen, J.Y., Funk, W.D., Wright, W.E., Shay, J.W., and Minna, J.D. (1993). Heterogeneity of transcriptional activity of mutant p53 proteins and p53 DNA target sequences. Oncogene *8*, 2159-2166.

Dhananjaya, B.L., and D'Souza, C.J. (2011). The pharmacological role of phosphatases (acid and alkaline phosphomonoesterases) in snake venoms related to release of purines - a multitoxin. Basic Clin Pharmacol Toxicol *108*, 79-83.

Dimri, G.P., Lee, X., Basile, G., Acosta, M., Scott, G., Roskelley, C., Medrano, E.E., Linskens, M., Rubelj, I., Pereira-Smith, O.*, et al.* (1995). A biomarker that identifies senescent human cells in culture and in aging skin in vivo. Proceedings of the National Academy of Sciences of the United States of America *92*, 9363-9367.

Donella Deana, A., Mac Gowan, C.H., Cohen, P., Marchiori, F., Meyer, H.E., and Pinna, L.A. (1990). An investigation of the substrate specificity of protein phosphatase 2C using synthetic peptide substrates; comparison with protein phosphatase 2A. Biochim Biophys Acta *1051*, 199-202.

Fujita, T., Kiyama, M., Tomizawa, Y., Kohno, T., and Yokota, J. (1999). Comprehensive analysis of p53 gene mutation characteristics in lung carcinoma with special reference to histological subtypes. Int J Oncol *15*, 927-934.

Hayashi, S., and McMahon, A.P. (2002). Efficient recombination in diverse tissues by a tamoxifen-inducible form of Cre: a tool for temporally regulated gene activation/inactivation in the mouse. Dev Biol *244*, 305-318.

Iwakawa, R., Kohno, T., Enari, M., Kiyono, T., and Yokota, J. (2010). Prevalence of human papillomavirus 16/18/33 infection and p53 mutation in lung adenocarcinoma. Cancer Sci *101*, 1891-1896.

Jagemann, L.R., Perez-Rivas, L.G., Ruiz, E.J., Ranea, J.A., Sanchez-Jimenez, F., Nebreda, A.R., Alba, E., and Lozano, J. (2008). The functional interaction of 14-3-3 proteins with the ERK1/2 scaffold KSR1 occurs in an isoform-specific manner. J Biol Chem *283*, 17450-17462.

Kashii, T., Mizushima, Y., Monno, S., Nakagawa, K., and Kobayashi, M. (1994). Gene analysis of K-, H-ras, p53, and retinoblastoma susceptibility genes in human lung cancer cell lines by the polymerase chain reaction/single-strand conformation polymorphism method. J Cancer Res Clin Oncol *120*, 143-148.

Kaufman, J.M., Yamada, T., Park, K., Timmers, C.D., Amann, J.M., and Carbone, D.P. (2017). A Transcriptional Signature Identifies LKB1 Functional Status as a Novel Determinant of MEK Sensitivity in Lung Adenocarcinoma. Cancer research *77*, 153-163.

Morita, S., Kojima, T., and Kitamura, T. (2000). Plat-E: an efficient and stable system for transient packaging of retroviruses. Gene Ther *7*, 1063-1066.

Nagai, Y., Miyazawa, H., Huqun, Tanaka, T., Udagawa, K., Kato, M., Fukuyama, S., Yokote, A., Kobayashi, K., Kanazawa, M*., et al.* (2005). Genetic heterogeneity of the epidermal growth factor receptor in non-small cell lung cancer cell lines revealed by a rapid and sensitive detection system, the peptide nucleic acid-locked nucleic acid PCR clamp. Cancer research *65*, 7276-7282.

Niida, H., Katsuno, Y., Banerjee, B., Hande, M.P., and Nakanishi, M. (2007). Specific role of Chk1 phosphorylations in cell survival and checkpoint activation. Mol Cell Biol *27*, 2572-2581.

Niwa, H., Yamamura, K., and Miyazaki, J. (1991). Efficient selection for high-expression transfectants with a novel eukaryotic vector. Gene *108*, 193-199.

Shreeram, S., Demidov, O.N., Hee, W.K., Yamaguchi, H., Onishi, N., Kek, C., Timofeev, O.N., Dudgeon, C., Fornace, A.J., Anderson, C.W*., et al.* (2006). Wip1 phosphatase modulates ATM-dependent signaling pathways. Molecular cell *23*, 757-764.

Notsuda, H., Sakurada, A., Endo, C., Okada, Y., Horii, A., Shima, H., and Kondo, T. (2013). p190A RhoGAP is involved in EGFR pathways and promotes proliferation, invasion and migration in lung adenocarcinoma cells. Int J Oncol *43*, 1569-1577.

Shreeram, S., Demidov, O.N., Hee, W.K., Yamaguchi, H., Onishi, N., Kek, C., Timofeev, O.N., Dudgeon, C., Fornace, A.J., Anderson, C.W*., et al.* (2006). Wip1 phosphatase modulates ATM-dependent signaling pathways. Molecular cell *23*, 757-764.

Song, X., Yu, Y., Shen, C., Wang, Y., and Wang, N. (2020). Dimerization/oligomerization of the extracellular domain of the GLP-1 receptor and the negative cooperativity in its ligand binding revealed by the improved NanoBiT. FASEB J *34*, 4348-4368.

Takeuchi, S., Takahashi, A., Motoi, N., Yoshimoto, S., Tajima, T., Yamakoshi, K., Hirao, A., Yanagi, S., Fukami, K., Ishikawa, Y*., et al.* (2010). Intrinsic cooperation between p16INK4a and p21Waf1/Cip1 in the onset of cellular senescence and tumor suppression in vivo. Cancer research *70*, 9381-9390.

Wei, S., Liu, T., Liu, H., and Gao, J. (2003). Unique GGT --> GTT mutation at K-ras codon 12 in six human pancreatic cancer cell lines from Chinese patients. Chin Med J (Engl) *116*, 1585-1587.